L-910900-16

Analytical Design and Performance Studies of the Nuclear Light Bulb Engine

NASA Contract No. SNPC-70

UNITED AIRCRAFT CORPORATION

United Aircraft Research Laboratories

EAST HARTFORD, CONNECTICUT

United Aircraft Research Laboratories

UNITED AIRCRAFT CORPORATION

EAST HARTFORD, CONNECTICUT 06108

L-910900-16

Analytical Design and Performance
Studies of the Nuclear
Light Bulb Engine

NASA Contract No. SNPC-70

REPORTED BY Richard J. Rodgers
Richard J. Rodgers

Thomas S. Latham
Thomas S. Latham

APPROVED BY James W. Clark
James W. Clark, Chief
Fluid and Systems Dynamics

DATE September 1972

NO. OF PAGES 73

COPY NO. 26

FOREWORD

An exploratory experimental and theoretical investigation of gaseous nuclear rocket technology was conducted by the United Aircraft Research Laboratories under Contract SNPC-70 with the joint AEC-NASA Space Nuclear Systems Office. The Technical Supervisors of the Contract for NASA were Captain C. E. Franklin (USAF) of SNSO for the initial portion of the Contract performance period, and Dr. Karlheinz Thom of SNSO and Mr. Herbert J. Heppler of the NASA Lewis Research Center for the final portions. The following nine reports (including the present report) comprise the required Final Technical Report under the Contract:

1. Roman, W. C. and J. F. Jaminet: Development of RF Plasma Simulations of In-Reactor Tests of Small Models of the Nuclear Light Bulb Fuel Region. United Aircraft Research Laboratories Report L-910900-12, September 1972.

2. Klein, J. F.: Nuclear Light Bulb Propellant Heating Simulation Using a Tungsten-Particle/Argon Aerosol and Radiation from a DC Arc Surrounded by a Segmented Mirror Cavity. United Aircraft Research Laboratories Report L-910900-13, September 1972.

3. Jaminet, J. F.: Development of a Model and Test Equipment for Cold-Flow Tests at 500 Atm of Small Nuclear Light Bulb Configurations. United Aircraft Research Laboratories Report L-910900-14, September 1972.

4. Kendall, J. S. and R. C. Stoeffler: Conceptual Design Studies and Experiments Related to Cavity Exhaust Systems for Nuclear Light Bulb Configurations. United Aircraft Research Laboratories Report L-910900-15, September 1972.

5. Rodgers, R. J. and T. S. Latham: Analytical Design and Performance Studies of the Nuclear Light Bulb Engine. United Aircraft Research Laboratories Report L-910900-16, September 1972. (Present Report)

6. Latham, T. S. and R. J. Rodgers: Analytical Design and Performance Studies of Nuclear Furnace Tests of Small Nuclear Light Bulb Models. United Aircraft Research Laboratories Report L-910900-17, September 1972.

7. Krascella, N. L.: Spectral Absorption Coefficients of Argon and Silicon and Spectral Reflectivity of Aluminum. United Aircraft Research Laboratories Report L-910904-3, September 1972.

8. Palma, G. E.: Measurements of the UV and VUV Transmission of Optical Materials During High-Energy Electron Irradiation. United Aircraft Research Laboratories Report L-990929-3, September 1972.

9. Kendall, J. S.: Investigation of Gaseous Nuclear Rocket Technology -- Summary Technical Report. United Aircraft Research Laboratories Report L-910905-13, September 1972.

Report L-910900-16

Analytical Design and Performance Studies of the Nuclear Light Bulb Engine

TABLE OF CONTENTS

	Page
SUMMARY	1
RESULTS AND CONCLUSIONS	2
INTRODUCTION	4
BASIC NUCLEAR LIGHT BULB REFERENCE ENGINE DESIGN	6
ENGINE HEAT LOADS	8
Fission Energy Deposition	8
Radiant Heat Transfer	10
Spectral Flux Calculations	11
Buffer-Gas Heating	13
Thermal Radiation Absorption in Transparent Walls	16
Thermal Radiation Absorption by Liner Surfaces	17
Conduction and Convection Heat Transfer	18
Reference Heat Loads and Cooling Sequence	20
CHARACTERISTICS OF ENGINE COOLANT CIRCUITS	22
Secondary Hydrogen Circuit	22
Space Radiator Circuit	23
Fuel-Neon Separator Circuit	23
Fuel and Silicon Seed Injection	24
Primary Hydrogen Propellant Circuit	26
ENGINE DYNAMICS AND PERFORMANCE	27
Dynamic Response of Engine	27
Engine Performance	28

TABLE OF CONTENTS (Continued)

	Page
REFERENCES	29
LIST OF SYMBOLS	33
TABLES	37
FIGURES	52

Report L-910900-16

Analytical Design and Performance Studies of the Nuclear Light Bulb Engine

SUMMARY

Analytical studies were conducted to investigate in detail the heat balance characteristics of the nuclear light bulb engine. Distributions of energy deposition to all engine components from the fission process, conduction and convection, and thermal radiation were considered. Where uncertainties in basic data or heat transfer characteristics were encountered, ranges of heat loads were calculated and reference values were selected. The influence of these heat loads on engine performance, space radiator requirements, and cooling sequence and cooling circuit designs was determined.

Reference heat balance conditions were chosen which resulted in an engine with a weight of 37,250 kg (82,000 lb), including a space radiator weight of 5500 kg (12,100 lb); a thrust of 409,000 N (92,000 lb); and a specific impulse of 1870 sec. The space radiator serves a dual purpose -- rejection of 118 MW of power from structural components of the system during steady-state operation and rejection of fission product decay heat and sensible heat from bulk moderator and structural components after engine shutdown.

The analyses resulted in revisions to the previously reported reference engine characteristics, principally in the heat loads to some engine components and in the cooling sequence. These revisions were incorporated in the engine dynamics digital computer simulation program. No significant changes occurred in the dynamic response of the engine to perturbations in fuel injection rate, reactivity or exhaust nozzle area.

RESULTS AND CONCLUSIONS

1. Based on the most recent calculations of thermal radiation, conduction, convection, and nuclear radiation heat loads, the nuclear light bulb reference engine has the following performance characteristics: engine power level, 4600 MW; operating pressure, 500 atm; engine weight, 37,250 kg (82,000 lb); thrust, 409,000 N (92,000 lb); specific impulse, 1870 sec; and thrust-to-weight ratio, 1.12. The principal change from previously calculated engine performance is in the total engine weight, which has been increased from 31,750 kg to 37,250 kg to allow for the addition of a 5500-kg (12,100-lb) space radiator. The space radiator serves the dual purpose of rejecting 118 MW of power from structural components of the system during steady-state operation and rejecting fission product decay heat and sensible heat from bulk moderator and structural components after engine shutdown. It is located in the secondary hydrogen coolant circuit and operates at rejection temperatures ranging from 833 to 389 °K.

2. Calculations of spectral heat fluxes emitted from the fuel region were made for the reference engine for several partial pressures of silicon seed in the edge-of-fuel and buffer-gas regions. Results of these calculations indicate that, with 10 atm of silicon seed in the aforementioned regions, the fraction of uv radiation at wavelengths below 0.18μ emitted from the nuclear fuel cloud is approximately 0.002. Combined conduction and thermal radiation absorption in the buffer-gas region results in the buffer-gas flow convecting away 3.6 MW per cell, or 25.2 MW for all seven cells. The required neon weight flow to remove this energy ranges from 1.75 to 12.4 kg/sec (3.85 to 27.3 lb/sec) per cell, depending upon the buffer-gas flow configuration employed at the cavity end walls.

3. The heat loads in the transparent walls due to nuclear radiation absorption, ultraviolet radiation absorption at wavelengths shorter than the uv cutoff in fused silica, and thermal radiation absorption due to nuclear-induced coloration are 14.7, 1.9 and 1.1 MW, respectively (a total of 17.7 MW) when 10 atm of silicon seed is employed in the edge-of-fuel and buffer-gas regions.

4. The position of the secondary circuit heat exchanger and the fuel cycle heat exchanger in the reference engine flow schematic has been reversed for the following reasons: (1) the convection heat loads on the propellant channel liners and the cavity end wall heat loads have been revised upward such that a greater low-temperature heat sink is required to maintain the temperature of those components at acceptable levels; and (2) a different fuel/buffer-gas separator (one in which the fuel must be in liquid droplets) was used, requiring that the fuel cycle heat exchanger operate between approximately 1500°K and 800°K, and that the fuel circuit reject its heat at a higher temperature than previously.

5. Several options for injecting nuclear fuel into the fuel cavity were investigated. The most promising were (1) injection of a uranium-silicon eutectic in liquid form and (2) injection of UF_6 in liquid form. Use of the eutectic would possibly eliminate the need to inject silicon seed with the neon buffer gas. Use of UF_6 would be combined with injection of silicon with the neon buffer gas by adding gaseous, colorless silicon tetrafluoride to the neon. Further investigations of these options are required.

6. The revised heat loads throughout the nuclear light bulb engine were incorporated in the engine dynamics simulation program. The response of the engine to perturbations in reactivity, fuel flow rate, and exhaust nozzle area were essentially the same as previous responses calculated before the revisions in heat balance were incorporated.

INTRODUCTION

Investigations of various phases of gaseous nuclear rocket technology have been conducted at the United Aircraft Research Laboratories under Contract SNPC-70, administered by the joint AEC-NASA Space Nuclear Systems Office. Previous investigations were conducted under NASA Contracts NASw-847, NASw-768 and NAS3-3382; under Air Force Contracts AF 04(611)-7448 and AF 04(611)-8189; and under Corporate sponsorship.

The principal research effort is presently directed toward the closed-cycle, vortex-stabilized nuclear light bulb engine. This engine concept is based on the transfer of energy by thermal radiation from gaseous fissioning uranium, through a transparent wall, to hydrogen propellant. The basic design is described in detail in Ref. 1. Subsequent investigations which were performed to supplement and investigate the basic design and to investigate other phases of nuclear light bulb engine component development are reported in Refs. 2 through 15. Reference 16 contains a summary of nuclear light bulb research conducted under Contract SNPC-70 through September 1972.

The majority of engine design work performed prior to FY 1969 was concerned with the component design and operating characteristics of the nuclear light bulb engine operating at full-power, steady-state conditions. During the FY 1969 contract period, a digital computer simulation model was formulated for the purpose of investigating the transient response of the reference engine to perturbations about the full-power, steady-state design conditions. This engine dynamics model is described in detail in Ref. 3. In addition to the dynamic response studies, preliminary investigations of engine start-up and shutdown procedures and the operating conditions and control systems required during these phases of operation were performed. These investigations were all based on the reference engine described in Ref. 1 with modifications which evolved subsequently. These latter studies were conducted during the FY 1970 and 1971 contract periods and are described in Refs. 5 and 7.

Since the time of the determination of the characteristics of the reference nuclear light bulb engine described in Ref. 1, considerable research has been performed which has resulted in modifications to several of the component heat loads and the general heat balance throughout the engine. In particular, the spectral absorption properties of the transparent-wall materials have been measured during irradiation by an electron beam with a similar ionizing dose rate to that expected in the reference engine. The results of these measurements have indicated that the absorption of radiant energy by the transparent walls due to nuclear-radiation-induced coloration will be less than was anticipated. Detailed calculations of the spectral heat flux expected to be emitted from the fuel region have also been performed and have led to revisions of the fraction of uv energy which is expected to

be absorbed by the transparent walls. Other characteristics have also changed, such as the expected average fuel residence time and the range of radiation heat loads on the fuel region end walls and on the propellant channel liners. In addition, it was determined that a space radiator would be required to remove the decay heat from fission products and the sensible heat in the bulk moderator region after shutdown. The space radiator, therefore, is available for removal of some part of the engine heat load during steady-state operation.

The objectives of the work described in the present report were to (1) incorporate the most recent information on the fuel recirculation system, the heat loads on the liner components in the engine, the radiant heat transfer characteristics in the fuel region, and the space radiator into the operating characteristics and design of the reference engine, and (2) to calculate the effects of these changes on the engine and its dynamic response.

BASIC NUCLEAR LIGHT BULB REFERENCE ENGINE DESIGN

The reference nuclear light bulb engine design which has resulted from previous studies has the following characteristics:

1. Cavity configuration -- seven separate, 1.83-m-long (6-ft-long) cavities having a total overall volume of 4.8 m^3 (170 ft^3)

2. Cavity pressure -- 500 atm

3. Specific impulse -- 1870 sec

4. Total propellant flow (including seed and nozzle transpiration coolant flow) -- 22.4 kg/sec (49.3 lb/sec)

5. Thrust -- 409,000 N (92,000 lb)

6. Engine power -- 4600 MW

7. Engine weight -- 31,750 kg (70,000 lb)

8. Ratio of average density in fuel-containment region to neon density at edge of fuel -- 0.7

Sketches illustrating the principle of operation of the engine are shown in Fig. 1. Energy is transferred by thermal radiation from gaseous nuclear fuel contained in a neon vortex (Fig. 1(b)) to hydrogen propellant seeded with tungsten particles to increase its opacity. The vortex and propellant regions are separated by an internally-cooled fused silica transparent wall. A seven-cavity configuration (Fig. 1(a)) is employed in the reference engine, rather than one large single cavity, to increase the total surface radiating area at the edge of the fuel for a given total cavity volume.

A schematic diagram of the current engine flow circuits is shown in Fig. 2. Neon is injected from the transparent wall to drive the vortex, passes axially toward the end walls, and is removed through ports at the center of one or both end walls (Fig. 1(b)). The hot gaseous mixture discharging from the cavity, consisting of neon, uranium vapor, fission-product vapors and silicon vapor (introduced with the buffer gas to protect the wall from uv radiation), is cooled in the neon and fuel cycle circuit (Fig. 2) by mixing with low-temperature bypass neon. This causes condensation of the nuclear fuel to liquid form. The condensed fuel is centrifugally separated from the neon and is collected in a fuel crucible zone (not shown separately in Fig. 2). Here, the nuclear fuel and silicon seed mixture is processed and prepared for re-injection into the cavity using one of several options, depending upon the forms of the fuel and seed (i.e., UF_6, U-Si eutectic, silicon

particles, etc.). The neon is cooled by rejecting heat to the primary hydrogen propellant, and is then pumped back to drive the vortex. Details of the fuel and neon separator are described later in this report and in Ref. 11.

The seven cavities are surrounded by a beryllium oxide moderator region (Fig. 1(a)) which fills the interstitial zones. The beryllium oxide region is surrounded by an annular graphite moderator region. These two axial moderator regions are separated by an internally-cooled flow divider which separates the flow in the two zones. The moderator is supported by 24 beryllium tie-rods which pass through the moderator region. In addition to the axial moderator regions, there are upper- and lower-end moderator regions which form the ends of the cavity. These end-moderator regions consist of a beryllium oxide region, which is adjacent to the cavity end walls, and a graphite region. The heat deposited in the moderator by neutron and gamma-ray heating and the heat transferred to the moderator and structure by conduction, convection and radiation is transferred to the primary hydrogen propellant before it enters the cavity (see primary and secondary hydrogen circuits in Fig. 2).

Several of the structural components, such as the beryllium tie-rods and flow divider and the cavity liner tubes, must be maintained at low temperatures to insure their structural integrity. These components are cooled by a secondary hydrogen coolant loop (see Fig. 2) which rejects its heat to low-temperature hydrogen from the hydrogen storage tanks. A space radiator is required to reject the fission fragment decay heat and to cool down the bulk moderator regions and structure after engine shutdown. This space radiator is available for use during full-power operation as well. The space radiator is coupled to the secondary coolant loop by a heat exchanger located after the transparent wall (see Fig. 2). The secondary coolant circuit is needed to limit pressure drops across structural and liner components. Cooling of these components could not be accomplished with the primary hydrogen, because it is pumped up to a pressure of 740 atm by the primary hydrogen pump to drive the turbopump system. An auxiliary loop is shown in the space radiator system which passes through the fuel and neon separator. This loop is activated after shutdown so that the fission product decay heat from the nuclear fuel collected in the separator can be rejected from the space radiator.

The distribution of heat deposition throughout the system resulting from the most recent calculations of thermal radiation, conduction, convection and nuclear radiation energy deposition modes have resulted in a modification to the reference engine cooling sequence. These modifications, which were described above, have all been incorporated in Fig. 2 and will be discussed in detail in the subsequent sections.

ENGINE HEAT LOADS

This section of the report discusses the primary results of additional calculations to estimate the heat loads in the components of the reference engine. There are four subsections:

1. Fission Energy Deposition -- heat loads in the components due to energy deposition by fission fragments, neutrons, and prompt gamma rays emitted at the time of fission, and by delayed gamma rays and beta particles emitted from fission fragments subsequent to the fission event.

2. Radiant Heat Transfer -- heat loads in the buffer gas and transparent walls due to absorption of thermal radiation from the fuel region (includes discussion of the effect of silicon seed in the edge-of-fuel and buffer-gas regions on the heat loads), and radiation heat loads on the liner surfaces which bound the propellant ducts and the cavity end walls.

3. Conduction and Convection Heat Transfer -- heat loads due to convection across the interfaces of the propellant stream with the transparent walls and liners which bound the propellant duct, due to transport of energy to the neon and fuel circuit by the mixture of hot gases exhausting from the cavities, and due to conduction from the fuel region to the buffer gas.

4. Reference Heat Loads and Cooling Sequence -- heat loads and cooling sequence used for calculating reference engine performance and operating characteristics.

Fission Energy Deposition

Energy is released by fission fragments, neutrons and prompt gamma rays emitted at the time of fission, and by delayed gamma rays and beta particles emitted from fission fragments subsequent to the fission event. The fractions of total energy released in the fission process are shown in Fig. 3, which contains a table of the energetics of U-233 fission and curves of the buildup with time of delayed energy release from fission fragments by beta particles and gamma rays. The data in Fig. 3 for delayed energy release by beta decay and gamma-ray emission from fission fragments were taken from experimental measurements reported in Refs. 17 and 18.

The rate of energy release by fission fragment decay is a complicated function of engine power level, operating time, and the concentrations and half-lifes of the various fission fragment species. The variation of decay heating from U-235 fission

fragments with operating time for a power level of 4600 MW for the reference nuclear light bulb engine is shown in Fig. 4. The curve in Fig. 4 was taken from Ref. 19. It was assumed that the decay heating from U-233 fission fragments would be essentially the same as that for U-235.

It can be seen that the fraction of the total engine power due to energy release by fission fragments, neutrons, and prompt gamma rays will differ relative to delayed energy release with operating time. These variations in the distribution of fission energy release at different operating times are shown in Table I. The ratio of delayed gamma-ray energy release to delayed beta particle energy release in Table I was based on the ratios of integrated delayed energy release from the curves of Fig. 3 at the specified times after fission. For purposes of establishing reference heat balance conditions for the nuclear light bulb engine, the distribution of fission energy release at an operating time of 1000 sec was chosen.

In the nuclear light bulb engine, moderator and structural components are heated by neutron and gamma-ray energy deposition. For the most part, gases are heated by fission fragment and beta particle energy deposition. The distribution of energy deposition is dependent on the ratio of residence time of the nuclear fuel in the active core to the residence time of the nuclear fuel and associated fission fragments in the neon-fuel separator. A summary of the rate of fission energy deposition in various principal components of the nuclear light bulb engine is given in Table II. In preparing this table it was assumed that the engine operating time was 1000 sec, the average fuel residence time in the active core was 4 sec, and the fuel circulation time through the neon-fuel separator and recirculation system was 16, 40 or 80 sec.

Whether the fission fragments were separated from the nuclear fuel in the separator or whether they continued to circulate with the fuel was calculated. Fission energy from the fuel buffer-gas mixture in the thru-flow ports as well as in the separator were also calculated and included in Table II. It can be seen from Table II that the principal variation in fission energy deposition results from delayed beta particle energy release in the separator and fission fragment energy deposition in the separator as the fuel circulation time varies. The deposition of energy throughout the system as a function of the separation efficiency of fission fragments from the nuclear fuel does not seem to vary significantly between cases with total separation and those with no separation at all, with the exception of the variation in the beta particle energy deposition in the separator. Since it is desirable to minimize the number of critical masses circulating through the separator, the circulation time of 16 sec with no separation of fission fragments from the nuclear fuel was chosen as the reference case for evaluating system heat loads.

Neutron and gamma heating in the various engine components is summarized in Table III. The deposition rates of neutron and gamma energy in the nuclear light bulb reference engine were calculated in detail in Ref. 2. The energy deposition

rates shown in Table III have the same distribution by component as that reported in Ref. 2, the differences being in the slight increase in total delayed gamma energy release for an operating time of 1000 sec. It can be seen from Table III that the neutron and gamma heating throughout the system is not affected significantly by the efficiency of the separator system in separating fission fragments from the nuclear fuel. In evaluating delayed gamma heating, it was assumed that the gamma rays released in the separator deposited 20 percent of their energy in the separator structure and that the remaining 80 percent was distributed throughout the engine in the same distribution as that for prompt gamma rays.

Radiant Heat Transfer

Approximately 90 percent of the energy deposition by fission occurs in the fuel-containment regions of the seven unit cavities. This energy is emitted in the form of thermal radiation from the nuclear fuel and is subsequently transmitted through both the neon buffer-gas layer and the internally-cooled transparent walls to seeded hydrogen propellant streams. To achieve maximum efficiency in this transfer of energy, it is necessary to minimize the absorption of radiant energy by the buffer gas and the transparent wall. The transparent wall is fabricated of fused silica which absorbs ultraviolet radiation at wavelengths shorter than approximately 0.18μ. Therefore, it is desirable to tailor the spectrum of thermal radiation emitted from the fissioning plasma such that the amount of uv radiation at wavelengths shorter than 0.18μ is minimized.

Elimination of most of the uv radiation can be accomplished by introducing seed gases at low partial pressures into the edge-of-fuel and buffer-gas regions. Past analytical studies of Refs. 7, 20 and 21 have indicated that a uranium plasma radiating at a power level corresponding to the 4600 MW reference engine power would contain some 14 to 18 percent of the total thermal radiation in the range of wavelengths shorter than the 0.18μ uv cutoff for fused silica.

Various seed gases (see Refs. 7, 20 and 21) have been evaluated to determine their effectiveness in minimizing the uv radiation. The calculations reported herein are based on the use of silicon seed which is shown to be very effective in reducing the amount of ultraviolet radiation emitted from the fuel region. However, the introduction of seed gases in the edge-of-fuel and buffer-gas regions does cause absorption of some thermal radiation in the buffer gas. This absorbed energy must be convected from the buffer-gas region with the neon flow. Therefore, it is necessary to determine not only the best seed gas for reducing the uv radiation, but also the concentration of seed gas which minimizes the absorption of radiation by the buffer gas while the energy deposition in the transparent wall material is held to a satisfactory level.

Spectral Flux Calculations

Calculations of spectral heat fluxes emitted from the nuclear fuel cloud of the nuclear light bulb reference engine were performed using the one-dimensional neutron transport theory computer code, ANISN (Ref. 22). Modifications to this program were made and incorporated into the radiant heat transfer analyses described in Ref. 7. The heat balance in the buffer-gas region and the radiant heat transfer calculations are based on the flow configuration shown in Fig. 5. Buffer gas is injected tangentially into the buffer-gas region and flows axially to the end of the vortex chamber in stream tubes which turn at different radial locations as the buffer gas proceeds radially inward. Shown in Fig. 5 are several radial locations of importance. The first radial surface in the buffer-flow region is the edge-of-fuel surface -- denoted by R_2, the location at which the fuel partial pressure is assumed to go to zero. Inside the edge-of-fuel location is a radial stagnation surface, which is an assumed radial location at which the net flow of buffer gas is zero. This radial stagnation surface model was developed from many radial inflow fluid mechanics tests reported in Refs. 23 and 24. The region of analysis for the radiant heat transfer calculations extends inward beyond the radial stagnation surface into the fuel region so that, at any wavelength, the optical depth, i.e., the number of radiation mean-free paths into the fuel region is greater than one. The innermost dashed line in Fig. 5(b) depicts the inner boundary of the radiant heat transfer region of analysis. The only fluid dynamic constraint on the flow in this model is a requirement that the axial dynamic pressure be constant with radius. This constraint then defines the axial velocity of the flow at each radial station and, as such, is a function of local temperature, density, and the specified constant axial dynamic pressure.

Typical fuel, seed and buffer-gas radial partial pressure distributions which were employed in the radiant heat transfer calculations are shown in Fig. 6. The total pressure in the system is 500 atm. The silicon seed partial pressure was assumed to vary over the range from 0 to 10 atm in the edge-of-fuel and high-temperature region of the buffer gas. In zones of the buffer-gas region where the temperature was low enough to condense silicon, the partial pressure of silicon was assumed to follow its vapor pressure curve. It can be seen from Fig. 6 that, at all stations, the total pressure is equal to the sums of the fuel, neon and seed partial pressures.

Spectral absorption coefficients for the mixtures of fuel, seed and buffer gas are required to perform the radiant heat transfer calculations. The compositions of the various materials and their spectral absorption coefficients are reported in Ref. 14. Figure 7 shows a typical variation of spectral absorption coefficient for uranium and silicon seed at a temperature of 10,000 °K. It can be seen that silicon has large absorption coefficients in the range from 50,000 to 140,000 wave numbers and that, in particular, silicon provides high absorption coefficients in the range from 70,000 to 80,000 wave numbers where there is a window in uranium spectral absorption coefficients. It is this window in the uranium which allows

ultraviolet radiation to stream out from high temperature zones in the fissioning plasma. This results in the high fractions of uv radiation (14 to 18 percent of the thermal radiation flux) which are calculated for a plasma consisting of uranium and neon buffer gas only. The neon buffer-gas spectral absorption coefficients are relatively insignificant in the edge-of-fuel and buffer-gas regions. However, the spectral absorption coefficients for neon are included in the analyses, and their values are reported in Ref. 25.

The calculated temperature distributions for the reference engine with various silicon seed partial pressures in the edge-of-fuel and buffer-gas regions are shown in Fig. 8. In the present analysis, the temperature distribution is flat over most of the outer region of the buffer gas. To help stabilize the buffer flow in this region, it is necessary to have a decreasing temperature distribution in the buffer-gas region out to the transparent walls. The reason for the flat temperature distribution is that the vapor pressure of silicon is rapidly decreasing as the temperature decreases and hence there is insignificant radiant energy absorption either by the silicon present or by the neon buffer gas. This results in a value of dT/dr which is essentially zero in the outer region of the buffer gas. However, there is some beta heating in the buffer gas on the same order of magnitude as the total convected energy presently calculated for the buffer-gas region. This beta-heating occurs over the entire buffer-gas region and, therefore, its inclusion in future analyses will result in a decreasing temperature distribution in the presently flat portion of the temperature distribution. The spectral heat fluxes at the edge-of-fuel location which correspond to these temperature distributions are shown in Fig. 9. With no seed present, uv radiation at about 75,000 wave numbers and 120,000 wave numbers streams through the edge-of-fuel region into the buffer-gas region, and creates a potentially large heat load in the transparent wall. With increasing partial pressure of silicon, the high spectral absorption coefficients cause the uv radiation to be absorbed by the silicon. The silicon relaxes its energy by collisions in the fuel and buffer-gas mixture and the absorbed energy is re-emitted by fuel atoms at wavelengths characteristic of the local temperature (the visible part of the spectrum). Put another way, the uv energy absorbed by the silicon cannot be reradiated readily by the silicon because the local temperature in the edge-of-fuel is too low. Collision times in the edge-of-fuel environment (500 atm, 8000-20,000 °K) are on the order of 10^{-12} sec compared with optical radiation lifetimes on the order of 10^{-9} sec, thereby allowing 10^3 collisions between the excited silicon atoms and nuclear fuel atoms before natural reradiation is apt to occur.

The fractional flux distributions which correspond to the spectral fluxes in Fig. 9 are shown in Fig. 10. With no silicon seed, approximately 14 percent of the thermal radiation is emitted at wavelengths less than 0.18μ. The decrease in fractional flux at wave numbers greater than 55,000 cm^{-1} or at wavelengths less than the 0.18μ fused silica uv absorption cutoff is shown in Fig. 10 as silicon seed partial pressure is increased. With 10 atm of silicon seed, the fractional flux for $\lambda < 0.18\mu$ is approximately 0.002.

In analyzing the spectral flux emitted from hot plasmas with steep temperature gradients at their boundary, a useful parameter is the optical depth at various wave numbers. The optical depth is defined as

$$\tau_\omega = \int_0^{\Delta R} a_\omega \, dR \qquad (1)$$

where ΔR is the radial distance from the edge-of-fuel location and a_ω is the spectral absorption coefficient at a given wave number, ω. Typically, the spectral radiation flux in a given wave number range will equal that of a black-body at the local temperature one optical depth into the steep temperature gradient. For a case with only uranium and neon in the plasma, the spectral flux shown in Fig. 9 indicates a peak in the uv radiation streaming out of the fission plasma in the wave number interval between 72,500 and 75,000 cm^{-1}. Optical depth distributions in the wave number interval from 72,500 to 75,000 cm^{-1} are shown in Fig. 11 for silicon partial pressures in the edge-of-fuel region from 0.0 to 10.0 atm. In that wave number range, the optical depth of the plasma equals 1.0 about 0.625 cm in from the edge-of-fuel location where the local temperature is approximately 13,200 °K. The addition of silicon seed reduces the radial distance into the plasma at which the optical depth equals 1.0 such that, with a silicon partial pressure of 10.0 atm, the local temperature at one optical depth is nearly the same as the edge-of-fuel temperature. The resulting reduction in uv radiation emission was discussed above.

The spectral fluxes in Fig. 9 can also be translated in terms of effective black-body radiating temperatures over the wave number range of interest. These effective radiating temperatures are shown in Fig. 12. It can be seen from these curves that the addition of the silicon seed systematically reduces the effective black-body radiating temperature from the fissioning plasma above 55,000 wave numbers from temperatures on the order of 12,000 °K to temperatures less than the effective black-body radiating temperature of 8330°K.

Buffer-Gas Heating

The heat load in the buffer-gas region resulting from the addition of silicon seed was calculated for seed partial pressures over the range from 0 to 10 atm. These results are summarized in Table IV, where it is seen that the energy convected by the buffer gas is least for a silicon seed partial pressure of 10 atm, the level which has been adopted for the reference engine. Reducing the seed partial pressure below 10 atm allows more uv radiation to cross the boundary between the fuel and buffer-gas regions. Since the seed absorbs uv radiation efficiently, the buffer region absorbs all the residual uv radiation coming at it from the fuel region. Thus, the radiation absorption in the buffer gas increases with decreasing seed partial pressure in the range from 10 to 0.1 atm. For a partial pressure of 0.1 atm, approximately 10 times as much energy is absorbed in the buffer gas as for 10 atm.

The total energy transmitted to the buffer gas includes both the thermal radiation absorption and the heat conducted from the nuclear fuel region. Since the temperature gradient in the edge-of-fuel region is fairly constant over the range of seed partial pressures studied (Fig. 8), the energy conducted into the buffer gas did not vary with seed partial pressure (Table IV).

The variation of integrated convected, conducted and absorbed energy with radius is shown in Fig. 13 for the case with 10 atm of silicon seed. Most of the energy absorption occurs within approximately 1 cm of the edge of fuel. The remaining part of the buffer-gas region out to the transparent wall has very little heat load burden. Consequently, the temperature distribution in the buffer gas tends to be quite flat from the transparent wall to within about 1 cm of the edge-of-fuel location. This feature was also shown in the temperature distribution in Fig. 8.

The radial weight flow and axial velocity distributions for the 10-atm silicon seed case are shown in Fig. 14. The region of constant temperature calls for a large amount of radial weight flow between the transparent wall and approximately 1 cm from the edge-of-fuel location because the constraint of constant axial dynamic pressure requires that flow turn in stream tubes at every radial station. Thus, most of the axial flow of buffer gas sees no heat load burden. For this flow configuration, the total radial weight flow per cell required to convect the heat absorbed by the buffer gas is 12.4 kg/sec.

Consideration must also be given to the stability of vortex flows with superimposed axial velocities that are large, as in the edge-of-fuel region. Flow stability criteria for radial-inflow vortexes were discussed in Refs. 26 and 27. A Richardson number criterion for rotating flow derived in Ref. 26 is

$$\mathrm{Ri} = \frac{V_{\phi_1}^2 \left(\frac{r}{r_1}\right)^{2n} \cdot \left(\frac{1}{r^2}\right) \left[\frac{r}{\rho}\frac{\partial \rho}{\partial r} + 2(n+1)\right]}{\left(\frac{\partial V_Z}{\partial r}\right)^2} \geq 0.25 \qquad (2)$$

In Eq. (2), V_{ϕ_1} is the average tangential velocity at the transparent peripheral wall, $\partial\rho/\partial r$ is the local radial gradient of total density, $\partial V_Z/\partial r$ is the axial shear (i.e., the local radial gradient of axial velocity), and the exponent n characterizes the tangential velocity profile (n = -1 is a free vortex; n = +1 is solid body rotation). Qualitatively, the numerator in Eq. (2) is the stabilizing term due to buoyancy or density stratification. The denominator represents the kinetic energy available to feed small perturbations and cause an instability. Stability occurs for $\mathrm{Ri} \geq 0.25$.

Equation (2) can be applied using the temperature and velocity profiles shown in Figs. 8 and 14(b), respectively. By setting Ri = 0.25 in Eq. (2), one can calculate the minimum value of peripheral wall velocity for stability. For the range n = -1 to n = +1, this gives V_{ϕ_1} = 11 and 15 m/sec, respectively, as limits. These

limits are compatible with the reference engine flow requirements. The key point is that in general, the large destabilizing axial shears which occur in the edge-of-fuel region (as in Fig. 14(b)) are balanced by the strong stabilizing effect of the very large temperature gradients (as in Fig. 8).

It is desirable to reduce the buffer-gas weight flow into the thru-flow ducts to the range of 1.5 to 3.0 kg/sec per cell for good fuel containment. Two-component gas vortex experiments discussed in Refs. 28 and 29 have indicated that simulated-fuel containment increased as the simulated-fuel-to-buffer-gas weight flow ratio calculated for the flow through the thru-flow ducts increased. The total radial weight flow of buffer gas can be reduced, and the aforementioned ratio increased, by employing alternate flow configurations for the buffer-gas region as shown in Fig. 15. One configuration would allow the outer portion of the buffer gas to flow through an axial bypass annulus (Fig. 15(a)) instead of flowing down the end wall to the thru-flow port. Another configuration would employ injection of neon through a peripheral part of the end wall (as in Fig. 15(b)), thereby preventing the turning of buffer gas in the axial direction until it arrived at a radius closer to the edge of fuel. Figure 15(c) shows the reduction in total neon buffer flow through the thru-flow ports which results if the radial location for turning of the buffer flow destined to pass through the thru-flow ports is brought inward from the transparent wall. Two-component gas vortex tests with axial bypass have shown very good containment characteristics (see Ref. 29); therefore, the axial bypass configuration was chosen for calculating heat balance conditions for the reference engine in a subsequent section.

Calculations show that the total radial weight flow required to maintain the wall temperature at an acceptable limit is sensitive to the assumed position of the radial stagnation surface relative to the edge of fuel. If the stagnation surface is coincident with the edge of fuel, the radial buffer weight flow must go to zero at the edge-of-fuel location, leaving very little convection capacity in the last stream tube adjacent to the fuel region. It is this interval in the buffer gas immediately adjacent to the edge-of-fuel location that has the highest radiation absorption rate and, therefore, requires as much flow as possible. By moving the stagnation surface inside the edge-of-fuel location, additional radial weight flow can pass across the buffer-gas fuel boundary and more radial weight flow can turn in the axial direction in the stream tubes which are absorbing the most radiation.

The results of changes in the assumed position of the stagnation surface are shown in Fig. 16. Moving the stagnation surface in 0.2 or 0.3 cm from the edge-of-fuel location causes marked reductions in total radial weight flow required (Fig. 16(b)). The corresponding mixed-mean temperature rise of the buffer gas is shown in Fig. 16(a).

The actual position of the radial stagnation surface for the nuclear light bulb engine is not known; it will be inside the edge of fuel at a location determined by the detailed fluid mechanics associated with the balance between the outward diffusion of fuel and the inward flow of buffer gas. For the purpose of establishing reference engine buffer-gas flow rates, the location 0.3 cm inside the edge-of-fuel location was used.

Thermal Radiation Absorption in Transparent Walls

Spectral heat fluxes at the inner surface of the transparent walls calculated for silicon seed partial pressures from 0 to 10 atm are shown in Fig. 17. The spectral heat fluxes calculated for the case with 10 atm of silicon seed were employed to calculate the transparent-wall heat load due to absorption of uv radiation. The absorption of uv radiation is described by

$$Q_{uv} = \sum_i q_{\omega_i} \Delta\omega_i \left[1 - e^{-2a_{\omega_i} \Delta r_{EFF}} \right] A_{TW} \qquad (3)$$

where a_ω is the absorption coefficient for the fused silica, Δr_{EFF} is the effective thickness of the transparent wall material, q_ω is the spectral heat flux, $\Delta\omega$ is the wave-number-group width, and A_{TW} is the transparent-wall area. Spectral absorption coefficients for fused silica at temperatures of 295°K and 1073°K were obtained from Ref. 30 and are shown in Fig. 18. The uv absorption in fused silica occurs over the wavelength range from 0.152 to 0.222 μ (for wavelengths less than 0.152 μ, the uv radiation is blocked by silicon seed; for wavelengths greater than 0.222 μ, the absorption coefficient vanishes). This range was divided into seven wave number groups in the spectral heat flux calculations. These seven values of q_ω were used in Eq. (3). Additional absorption due to radiation-induced coloration in a wavelength band centered at 0.215 μ is discussed below.

The results of the uv radiation absorption calculations are shown in Fig. 19 for the two transparent-wall temperatures. The operating temperature of the fused silica and the uv spectral heat flux are expected to fall within the ranges shown. For the reference engine with 0.0127-cm (0.005-in.)-thick walls, the uv absorption for the highest transparent-wall temperature was 1.9 MW for all of the transparent-wall material in the engine. It is feasible to increase tube wall thickness with only moderate increases in the heat load in accordance with Fig. 19.

The spectral heat fluxes for the case with 10 atm of silicon seed in the buffer-gas and edge-of-fuel regions were also employed to calculate the radiant energy absorbed in the transparent walls due to induced coloration from radiation damage. Measured induced absorption coefficients from Ref. 31 were employed; the shape of

the absorption band was also taken from Ref. 31. The results of the calculations are shown in Fig. 20. For the reference engine conditions with a 0.0127-cm-thick wall and an induced absorption coefficient of 0.1 cm^{-1} (Ref. 31), the induced thermal radiation absorption in the fused silica was 1.1 MW for all of the transparent-wall material in the engine.

A summary of all of the transparent-wall heat loads is given in Table V. Both the uv absorption and the absorption due to radiation-induced coloration in fused silica are very small fractions of the total engine power level. Moreover, their contributions to the total transparent-wall heat load, relative to the heat load due to gamma and neutron energy deposition and convection from the propellant stream, is small. Because the contribution from induced absorption is so small, and also because the contribution from beta particle absorption is small (3.3 MW), it is no longer expected that a magnetic field would be required to protect the walls from these types of heating, as specified in Ref. 1.

Thermal Radiation Absorption by Liner Surfaces

Radiation heat loads to propellant channel liner materials can be varied by selecting different liner materials. The choice of transparent-wall liner material has two effects on the overall heat balance since the material chosen has both a maximum operating temperature and an average reflectivity for the incident radiation flux. For example, aluminum liners have an average reflectivity of approximately 0.91 and a maximum temperature limitation of approximately 830°K. Tungsten liners have a reflectivity of approximately 0.6 and a maximum operating temperature of approximately 2500°K. Another possible liner material is polycrystalline BeO which might have reflectivities above 0.9 and maximum operating temperatures of approximately 1670°K.

The temperature variation of the propellant in the propellant channels was calculated in Ref. 1 assuming a constant rate of enthalpy increase in the stream as the propellant passes axially along each unit cell. This temperature variation was then employed in Ref. 1 to calculate the radiation heat load to the propellant channel walls and the transparent-wall support struts as functions of the average reflectivities of the liners of those components. (See Fig. 6 of Ref. 1 for schematic drawings of propellant channels and transparent-wall support struts.) The results of these calculations indicate that the total radiation heat load on aluminum liners with a reflectivity of 0.91 would be approximately 100 MW on the surfaces of the outer cavity liner and the liner tubes protecting the three support struts for the transparent-wall array. If tungsten were employed as a liner material, the total radiation heat load would increase to about 510 MW, assuming an average reflectivity of 0.6.

The cavity end walls are exposed to radiation from the conically shaped end of the uranium plasma. Since the end walls are close to the uranium plasma, and since the radiation heat flux will be intense at that location, it was concluded that

the end-wall liner materials should be tungsten-coated graphite or tungsten-coated tungsten carbide. These liners should have a reflectivity close to that for tungsten (calculated in Ref. 1 to be equal to 0.6 for the spectral heat flux emitted from the nuclear fuel cloud). Assuming a view factor from the fuel cloud of 0.5 based on the conical shape of the end of the plasma, and assuming that the end wall is contoured such that radiation is reflected into the neon bypass or the propellant stream, the radiation absorbed by tungsten-coated end walls should amount to approximately 195 MW for the entire engine system. It will be shown later that removal of this heat can be accomplished by ducting the primary hydrogen across the back of the end-wall liners.

An alternate approach for cooling the upper cavity end walls might be to line them with internally-cooled fused silica similar to the transparent-wall geometry. In this case, the hydrogen propellant containing tungsten seed could be ducted behind the transparent wall and could then exit directly into the propellant channel without further seed addition.

It is also possible that more highly reflective materials, such as polycrystalline BeO, might be employed as an end-wall liner material. However, if the reflected energy goes directly back into the uranium plasma, the result will be to raise the edge temperature at the ends of the plasma and expose the end walls to a more intense radiation flux. It is doubtful whether even highly reflective end walls can significantly reduce the radiant energy absorbed below the 195 MW estimated for a tungsten-lined end wall. It will be shown later that the use of the tungsten end walls does not tax the cooling capacity of the primary hydrogen circuit. In fact, a heat load higher than 195 MW could be tolerated if the outlet temperature of the tungsten-lined material could go as high as 2500°K, a temperature commonly used in the solid-core rocket fuel element program.

On the basis of these analyses, the thermal radiation heat loads to the propellant channel liners and the cavity end-wall liners were set at 100 MW and 195 MW, respectively, for the engine heat balance calculations. A summary of the calculated thermal radiation heat loads on various engine components is given in Table VI.

Conduction and Convection Heat Transfer

Heat transfer by conduction is the principal mode of heat transfer between the fuel region and the buffer gas at their interface. A discussion of the magnitude of the energy conducted from the fuel to the buffer-gas region was described in the previous section on radiant heat transfer and buffer-gas seeding. Heat transfer by convection occurs principally between the hydrogen propellant stream and the transparent walls and liner walls which bound the propellant channels. It occurs also by transport of energy from the nuclear fuel region into the fuel-neon separator

by the mixture of buffer gas and fuel flowing into the thru-flow exhaust duct. Discussion of the convection of energy from the fuel and buffer-gas regions to the fuel-neon separator is contained in a subsequent section.

Convection of energy to surfaces surrounding a flowing stream can be estimated by the Stanton number analysis employed in Ref. 32. The Stanton number is given by

$$St = \frac{0.023}{(Re)^{0.2}\ (Pr)^{2/3}} \tag{4}$$

and

$$Re = \frac{W_P\ d_e}{\mu\ A_P} \tag{5}$$

where Pr = Prandtl number, W_p = propellant mass flow rate, μ = hydrogen propellant viscosity, A_p = propellant channel cross-sectional flow area, and d_e = effective diameter for an annular passage, where d_e is given by

$$d_e = 2\ (R_c - R_{TW}) \tag{6}$$

where R_c = cavity radius and R_{TW} = transparent-wall radius. The convective heat flux to the walls is given by

$$Q_{WP} = St\ \frac{W_P\ H_P}{A_P} \tag{7}$$

where H_p is the propellant enthalpy. Assuming a linear increase in propellant enthalpy with axial distance through the propellant channel and using the engine design conditions from Refs. 5 and 7, the calculated local values of Stanton number varied from 0.00290 to 0.00303, with an average value of 0.003. The local values of convective heat flux to the walls varied from 5.1 to 5.7 MW/m^2, with an average value of 5.57 MW/m^2. Experimental evidence was given in Ref. 32 which indicated that by controlling the boundary layer flow between the propellant stream and the surfaces of the propellant channel, the Stanton number can be reduced by a factor

of 3 to 10. The types of boundary layer control which would reduce this Stanton number include transpiration cooling, film cooling, and selective control of the tungsten seed density across the propellant channel flow. For purposes of establishing a reference condition for the nuclear light bulb engine, it was assumed that the Stanton number could be reduced by a factor of 3.

The calculated convection heat loads on the surfaces surrounding the propellant channel are shown in Table VII. It will be shown in a later section that these convection heat loads on the liners and transparent walls can be cooled by the secondary hydrogen circuit without exceeding the temperature limits of the materials. Should the Stanton number be reduced by more than a factor of 3, which is a possibility, the material temperatures will be maintained well below the tolerable temperature limits.

Reference Heat Loads and Cooling Sequence

The underlying philosophy in choosing the reference heat loads in this study was more conservative than in earlier nuclear light bulb heat balance studies. In particular, convection and thermal radiation heat loads to various surfaces in the engine are assigned higher reference values. It is shown, however, that there is adequate cooling capacity in the cooling circuits to maintain local temperature levels throughout the system at acceptable limits. Thus, with the present modifications, the constraints on performance of surface cooling techniques and/or on the reflecting qualities of surface liners are relaxed considerably over previous reference engine models.

Full-power, steady-state moderator and structure heat deposition rates are shown in Table VIII for the reference engine of Refs. 1 and 7, and for the engine with the modified heat loads from the present analyses. The rise in the percent of total power deposited in the various components of the engine can be attributed to (1) the buildup of delayed gamma ray and beta particle energy release after 1000 sec of operation and (2) the increases in convection and thermal radiation heat loads to various surfaces in the engine (these increases result primarily from relaxing assumptions about the surface cooling techniques and/or control of stream seeding to protect propellant channel liners). Of the 889.3 MW to be rejected from engine components, 56.6 MW goes into direct heating of the hydrogen propellant, 117.8 MW is rejected by the space radiator, and 37.5 MW goes into the turbopump to pressurize and pump the hydrogen propellant. This leaves 676.4 MW to be absorbed by the primary hydrogen propellant with a weight flow of 19.3 kg/sec, resulting in an exit temperature of 2264°K from the last cooled component (i.e., the temperature at the inlet to the propellant channel). It will be shown later that all components are maintained at acceptable temperature levels throughout the engine with the calculated heat loads shown in Table VIII.

Several factors have led to revision of the cooling sequence employed in previous heat balance studies:

(1) The fuel-neon separator and recirculation system has been designed such that the uranium remains in liquid form, thus requiring a high-temperature cycle.

(2) The increases in convection heat loads require greater low-temperature cooling capacity.

(3) A space radiator required to reject fission product decay energy and to remove sensible heat from large moderator regions after engine shutdown was available to also reject heat during steady-state operation.

These factors resulted in reversing the order in which the secondary coolant circuit and fuel-neon circuit are cooled by primary hydrogen. Formerly, the fuel-neon circuit was cooled first; now, the secondary coolant circuit is cooled first.

The space radiator is coupled to the secondary coolant circuit through a heat exchanger at the transparent-wall outlet. An auxiliary loop is added to the secondary coolant circuit after shutdown to remove fission product heat from the nuclear fuel collected in the fuel-neon separator. These features of the engine cooling sequence are shown in Fig. 2. Details of the individual circuits are described in the next section.

CHARACTERISTICS OF ENGINE COOLANT CIRCUITS

The principal coolant circuits in the nuclear light bulb engine are (1) the secondary hydrogen circuit, (2) the fuel-neon separator and recirculation circuit, (3) the space radiator circuit, and (4) the primary hydrogen propellant circuit. These circuits are described below, and the calculated flow conditions and temperature levels throughout the circuit for the reference heat load conditions are discussed.

Secondary Hydrogen Circuit

The secondary hydrogen circuit is shown in the engine flow diagram in Fig. 2 with the major components and the sequence of cooling included. The turbopump system is driven by a turbine which requires 740 atm hydrogen at a temperature of approximately 1100°K as an inlet flow condition. Certain structural parts of the engine require cooling at temperature levels less than 800°K. In addition, to prevent the use of thick-wall tubes, the pressure in several of the internally-cooled components should be as close to the chamber operating pressure of 500 atm as possible. Therefore, a secondary hydrogen coolant circuit is employed to cool these components which have thin-walled tubes and which need to be kept at low temperatures.

The various heat loads to the moderator and structural components and the convection and conduction and thermal radiation loads to various liners and transparent walls have been discussed previously. These heat loads are summarized in Tables V through VIII. They have been incorporated in the engine dynamics simulation computer program which calculates the local temperatures at both the inlet and outlet of principal engine components. The choices of reference heat loads were based on the capacity of the primary hydrogen circuit, the secondary cooling circuit and the fuel-neon circuit to cool the various components. The hydrogen flow rate in the secondary circuit is matched to the primary hydrogen propellant flow rate at 19.3 kg/sec. The temperatures at local stations throughout the secondary circuit are summarized in Table IX.

The secondary coolant loop was connected to the first heat exchanger in the primary hydrogen circuit due to the need to maintain temperatures at low values in the tie-rods, liner materials and pressure vessels. The summary of the outlet temperatures given in Table IX shows that the transparent-wall outlet temperature is on the order of 1000°K, and that the low temperature material outlet temperatures are all less than about 800°K.

As mentioned earlier, a space radiator is required to remove the sensible heat from moderator zones and to remove fission fragment decay heat after the engine has been shut down. This space radiator has been added to the secondary coolant loop downstream of the transparent-wall outlet and is employed during steady-state operation to remove 118 MW of power from the secondary hydrogen loop. The space radiator is coupled to the secondary loop across a heat exchanger (Fig. 2). An auxiliary loop (shown by dashed line in Fig. 2) is added to the secondary circuit after engine shutdown so that the secondary coolant flow can remove fission fragment decay heat from the nuclear fuel collected in the separator. The secondary loop continues to remove heat conducted from the bulk moderator regions to the components in the secondary circuit after shutdown, as described in Ref. 7.

Space Radiator Circuit

The capacity required for rejection of decay heat and sensible heat in the bulk moderator after shutdown was established by the maximum power due to fission products after run times up to 1500 sec (see Table IV of Ref. 7). The space radiator system weight for an aluminum radiator was 5500 kg. In the present system, it is assumed that a space radiator system with the same capacity would be employed for heat rejection during steady-state operation. The weight for the system would be, therefore, 5500 kg. The steady-state heat rejection rate would be 118 MW.

Fuel-Neon Separator Circuit

Neon bypass flow is added to the mixture exiting the cavity in the thru-flow ducts to cool and condense the uranium and silicon. The cooled mixture then enters a fuel-neon centrifugal separator (see results of conceptual design study in Ref. 11). After separation of neon from the nuclear fuel and silicon, the neon passes through the H_2-Ne heat exchanger and rejects its heat to the primary hydrogen. It is then pumped back into the cavity and bypass manifold.

The liquid nuclear fuel and silicon mixture is then removed to a high-temperature crucible zone configured to prevent critical masses of U-233 from accumulating by its geometric shape. The hold time of the liquid nuclear fuel and silicon mixture in the crucible zone is approximately 12 sec. During this time, the fuel and silicon is processed or separated for re-injection into the active core, depending upon the form in which the silicon seed is added to the cavity.

The fuel and neon mixture exiting the vortex region is at a temperature above the liquefaction point of uranium. The mixture is cooled down by adding neon bypass so that the temperature is controlled at 1500°K. At this temperature, the uranium

and silicon are condensed in small droplet and particle form for separation in the fuel-neon separator. During passage through the thru-flow duct there is release of energy by fission of the uranium which also has to be cooled by the addition of bypass flow. In addition, in the crucible zone there is both fission energy release and beta particle energy release.

The bypass flow rates and the local temperature conditions throughout the fuel recirculation system are summarized in Tables X and XI. The requirement to operate the fuel cycle at relatively high temperatures made it possible to reverse the position of the heat exchangers in the primary hydrogen circuit from previously reported reference engine flow diagrams. These general features are shown in the reference engine flow diagram in Fig. 2.

The primary hydrogen passes through a heat exchanger in the fuel-neon separator system (Fig. 2). Heat released in the high-temperature crucible zone is rejected to the primary hydrogen across that heat exchanger. Rejection of this energy directly to the primary hydrogen allows the H_2-Ne heat exchanger circuit to operate at lower temperatures than if the neon was also used to cool the crucible zone. This reduces the total neon weight flow requirements in the separator circuit.

The crucible zone is envisioned as an array of tungsten or internally-coated graphite tubes fed from the liquid fuel outlet of the fuel-neon separator. Each tube would be surrounded by hafnium-carbide poison material to isolate it neutronically and minimize fission heating of the liquid uranium. An array of six 2.54-cm-i.d., 85-cm-long tubes would store approximately 42 kg of U-233, the quantity expected to be contained in the crucible zone.

Fuel and Silicon Seed Injection

The processing of the uranium-silicon mixture in the high-temperature crucible zone depends upon the method of injecting silicon seed into the fuel and buffer-gas regions and the form in which silicon seed is transported into those regions. The options, which have not been studied in detail (particularly with respect to chemical considerations) are as follows:

(1) Do not separate the silicon from the nuclear fuel. Instead inject a Si-U eutectic solution as the fuel form. In this case, no seed would be injected with the buffer gas.

(2) Use UF_6 fuel with gaseous SiF_4 as the seed in the neon buffer gas.

(3) Separate the silicon from the nuclear fuel and react with hydrogen to form silane gas (SiH_4) which could be added to the neon buffer gas for injection into the fuel cavity.

(4) Separate the silicon from the nuclear fuel. Inject silicon with neon buffer gas only in the form of submicron-sized particles.

In the first option, the variation of optical depth with penetration distance into the nuclear fuel cloud shown in Fig. 15 was used to determine the variation of optical depth if silicon seed were added with the nuclear fuel instead of with the buffer gas. These optical depth curves are shown in Fig. 21. The results indicate that in the wave number range from 72,500 to 75,000 cm^{-1}, an optical depth of one can be reached in less than 0.1 cm penetration into the fuel cloud if silicon at 100 atm is mixed with the nuclear fuel, and if the assumption is made that the silicon partial pressure varies in proportion to the nuclear fuel partial pressure. This means that the spectral radiation emitted from the fuel cloud in this wave number range, with this method of adding seeds, would be of an intensity less than that from the engine equivalent black-body radiating temperature of 8333°K. Thus, instead of adding seed to the buffer gas, it appears possible to add seed to the nuclear fuel. This system of seeding would relieve the buffer gas of uv radiation absorption and would reduce the convection heat loads to the buffer gas to that from energy conducted from the fuel cloud exclusively. Typically, these heat loads were approximately 20 percent of the reference engine heat load when 10 atm of silicon seed was added to the buffer gas. Introducing silicon seed to the reference engine intimately mixed with the nuclear fuel would eliminate the need to separate the silicon seed from the nuclear fuel in the crucible zone of the separator system. The phase diagram for U-Si mixtures from Ref. 33 indicates that, in the range of 20 to 40 atom percent of silicon mixed with uranium, a eutectic liquid with U_5Si_3 particles exists at temperatures above 1250°K. Also, 40 atom percent silicon would amount to an average of 80 atm partial pressure of silicon in the fuel region. Further investigations of this means of injecting silicon seed and nuclear fuel should be conducted.

For the second option, uranium hexafluoride at high pressures could be injected as a liquid fuel. Transparent, gaseous silicon tetrafluoride with fluorine enrichment could be added to the neon as a buffer-gas constituent. The presence of silicon tetrafluoride and fluorine gas would cause any uranium diffusing toward the transparent walls to be reacted into a uranium fluoride form which, if the reaction went all the way to UF_6, would prevent deposition of uranium compounds on the transparent walls. The reaction rates for fluorine with uranium are reportedly very high at high temperatures. In addition, a precedent for the use of fluorine-rich gas to reduce thermal and nuclear radiation dissociation of UF_6 was reported in Ref. 34. In this experiment, an over-pressure of fluorine caused a retardation of the thermal and nuclear dissociation of UF_6 in a test capsule inserted in a nuclear reactor. Thus, a UF_6-SiF_4-fluorine system appears to be a compatible fuel, buffer gas and buffer-gas seed system which could be used for nuclear light bulb engines with a fairly simplified fuel recirculation system.

Engine operating pressure might be higher than 500 atm due to the dissociation of UF_6 in the fissioning plasma.

In option three, the use of silane appears attractive since hydrogen has also been shown to be effective in minimizing uv radiation at approximately 60,000 and 115,000 wave numbers (see Ref. 20). However, the chemistry of forming silane by passing hydrogen over the heated uranium-silicon mixture must be investigated.

In the fourth option, the liquid fuel and silicon would be allowed to heat up by fission fragment decay, principally beta particle energy release, to a temperature which would boil off the silicon and maintain the uranium in liquid form. The silicon would be distilled by flowing neon over the boiling mixture and transporting the gases to a cooler zone where the silicon would condense into small particles for re-injection into the cavity. The vapor pressure curves for silicon and uranium from Ref. 35 indicate that at elevated temperatures, the ratio of silicon-to-uranium vapor pressure is approximately 10^3. This would result in a level of uranium contamination in the seed flow which might cause significant visible radiation absorption in the buffer gas.

Primary Hydrogen Propellant Circuit

The primary hydrogen circuit consists of the hydrogen tank; a pump at the exit of the hydrogen tank which raises the hydrogen pressure from 1 atm at the tank outlet to 740 atm pressure; the secondary circuit and fuel-neon circuit heat exchangers; and the turbine (for pump drives). After exiting the turbine, the primary hydrogen is used to cool the bulk moderator zones of the engine and to cool the end-wall liners. After exiting the end-wall liners, the primary hydrogen has tungsten seed added to it and passes over the transparent walls to pick up the direct thermal radiation from the uranium plasma zones.

A summary of the temperatures at key stations in the primary hydrogen circuit is given in Table XII. The temperatures in this system do not exceed 1700°K in beryllium oxide regions, and do not exceed 2500°K in graphite regions. The region with the highest temperature is the cooling zone behind the upper end-wall liners. The end-wall liners, as described previously, are made of tungsten-lined graphite. It is assumed that these materials can be operated at temperatures similar to those demonstrated in the solid-core nuclear rocket program, i.e., $\leq 2500^{\circ}K$. The outlet temperature from the upper end-wall liner is 2264°K.

ENGINE DYNAMICS AND PERFORMANCE

Dynamic Response of Engine

The UNIVAC 1108 digital computer simulation program for calculating the dynamic response of the nuclear light bulb engine to various perturbations in engine parameters is described in detail in Refs. 3, 5, and 7. The variations in reference engine heat loads resulting from the studies reported herein were introduced in the engine dynamics program. These variations included interchanging the location of the secondary hydrogen and fuel-neon circuit heat exchangers and incorporating the upper and lower end-wall liners in the primary hydrogen circuit. The space radiator was also added to the secondary hydrogen loop, but did not have a transient response included in its behavior. The space radiator heat rejection rate should be a slowly varying function of the temperature at the outlet of the transparent wall. It was assumed that perturbations in that temperature would be reflected in the secondary hydrogen loop with long time lags after perturbations had settled out in the engine components. In addition, the components of the secondary coolant loop do not contribute significantly to the reactivity feedback coefficients in the system.

After the changes in heat loads and cooling sequence were incorporated in the program, perturbations in reactivity, fuel weight flow rate, and exhaust nozzle throat area similar to those reported in Ref. 7 were introduced. The dynamic responses of the engine to these perturbations were essentially the same as those calculated previously. This was expected since the only change to the major components of the system was the interchange of the two primary circuit heat exchangers. Basically, the temperatures and densities in the bulk moderator, propellant region and fuel region zones which have the major influence on stability and response of the engine were unchanged by this re-arrangement of heat exchangers.

To illustrate the correspondence between the dynamic response behavior of the two configurations, the responses of the reference engine to a 10-percent change in fuel injection flow is shown in Fig. 22. The open symbols show the response using the new reference engine cooling sequence, while the curve shows the response reported on Fig. 38 of Ref. 7. Similar correspondence was obtained for the other perturbations studied in Ref. 7.

Engine Performance

Engine performance characteristics of the reference engine have remained the same as those reported in Ref. 7 with the exception that the space radiator weight of 5500 kg has been added to the total system weight. This results in a reduction in thrust-to-weight ratio from 1.3 to 1.12. Table XIII contains an updated summary of engine performance characteristics.

REFERENCES

1. McLafferty, G. H. and H. E. Bauer: Studies of Specific Nuclear Light Bulb and Open-Cycle Vortex-Stabilized Gaseous Nuclear Rocket Engines. United Aircraft Research Laboratories Report F-910093-37, prepared under Contract NASw-847, September 1967. Also issued as NASA CR-1030.

2. Latham, T. S.: Nuclear Studies of the Nuclear Light Bulb Rocket Engine. United Aircraft Research Laboratories Report G-910375-3, prepared under Contract NASw-847, September 1968. Also issued as NASA CR-1315.

3. Latham, T. S., H. E. Bauer, and R. J. Rodgers: Studies of Nuclear Light Bulb Start-Up Conditions and Engine Dynamics. United Aircraft Research Laboratories Report H-910375-4, prepared under Contract NASw-847, September 1969.

4. McLafferty, G. H.: Investigation of Gaseous Nuclear Rocket Technology - Summary Technical Report. United Aircraft Research Laboratories Report H-910093-46, prepared under Contract NASw-847, November 1969.

5. Bauer, H. E., R. J. Rodgers, and T. S. Latham: Analytical Studies of Start-Up and Dynamic Response Characteristics of the Nuclear Light Bulb Engine. United Aircraft Research Laboratories Report J-910900-5, prepared under Contract SNPC-70, September 1970.

6. McLafferty, G. H.: Gas Core Nuclear Rocket Engine Technology Status. J. Spacecraft Rockets, vol. 7, no. 12, December 1970, pp. 1391-1396.

7. Rodgers, R. J., T. S. Latham, and H. E. Bauer: Analytical Studies of Nuclear Light Bulb Radiant Heat Transfer and Performance Characteristics. United Aircraft Research Laboratories Report K-910900-10, prepared under Contract SNPC-70, September 1971.

8. Roman, W. C. and J. F. Jaminet: Development of RF Plasma Simulations of In-Reactor Tests of Small Models of the Nuclear Light Bulb Fuel Region. United Aircraft Research Laboratories Report L-910900-12, prepared under Contract SNPC-70, September 1972.

9. Klein, J. F.: Nuclear Light Bulb Propellant Heating Simulation Using a Tungsten-Particle/Argon Aerosol and Radiation from a DC Arc Surrounded by a Segmented Mirror Cavity. United Aircraft Research Laboratories Report L-910900-13, prepared under Contract SNPC-70, September 1972.

REFERENCES (Continued)

10. Jaminet, J. F.: Development of a Model and Test Equipment for Cold-Flow Tests at 500 Atm of Small Nuclear Light Bulb Configurations. United Aircraft Research Laboratories Report L-910900-14, prepared under Contract SNPC-70, September 1972.

11. Kendall, J. S. and R. C. Stoeffler: Conceptual Design Studies and Experiments Related to Cavity Exhaust Systems for Nuclear Light Bulb Configurations. United Aircraft Research Laboratories Report L-910900-15, prepared under Contract SNPC-70, September 1972.

12. Bauer, H. E.: Status of Nuclear Light Bulb Engine Design and Performance Analysis. Second Symposium on Uranium Plasmas: Research and Applications, Georgia Institute of Technology, November 1971.

13. Latham, T. S. and R. J. Rodgers: Analytical Design and Performance Studies of Nuclear Furnace Tests of Small Nuclear Light Bulb Models. United Aircraft Research Laboratories Report L-910900-17, prepared under Contract SNPC-70, September 1972.

14. Krascella, N. L.: Spectral Absorption Coefficients of Argon and Silicon and Spectral Reflectivity of Aluminum. United Aircraft Research Laboratories Report L-910904-3, prepared under Contract SNPC-70, September 1972.

15. Palma, G. E.: Measurements of the UV and VUV Transmission of Optical Materials During High-Energy Electron Irradiation. United Aircraft Research Laboratories Report L-990929-3, prepared under Contract SNPC-70, September 1972.

16. Kendall, J. S.: Investigation of Gaseous Nuclear Rocket Technology - Summary Technical Report. United Aircraft Research Laboratories Report L-910905-13, prepared under Contract SNPC-70, September 1972.

17. Kutcher, J. W. and M. E. Wyman: An Experimental Study of the Time Dependence of the Beta Energy Spectrum from U-233 Fission Fragments. Nuc. Science Eng., vol. 26, 1966, p. 435.

18. Engle, L. B., P. C. Fisher, and M. P. Kellogg: Energy and Time Dependence of Delayed Gammas from Fission. Los Alamos Scientific Laboratory Report LAMS-2642, January 1962.

19. Untermyer, S. and J. T. Weills: Heat Generation In Irradiated Uranium. Argonne National Laboratory Report ANL-4790, Argonne National Laboratory, Chicago, Illinois, February 25, 1952.

REFERENCES (Continued)

20. Krascella, N. L.: Theoretical Investigation of the Radiant Emission Spectrum from the Fuel Region of a Nuclear Light Bulb Engine. United Aircraft Research Laboratories Report H-910092-12, prepared under Contract NASw-847, September 1969.

21. Krascella, N. L.: Analytical Study of the Spectral Radiant Flux Emitted from the Fuel Region of a Nuclear Light Bulb Engine. United Aircraft Research Laboratories Report J-910904-1, prepared under Contract SNPC-70, September 1970.

22. Engle, W. W., Jr.: A User's Manual for ANISN, A One-Dimensional Discrete Ordinates Transport Code with Anisotropic Scattering. Union Carbide Corporation Report K-1693, 1967.

23. Travers, A.: Experimental Investigation of Radial-Inflow Vortexes in Jet-Injection and Rotating-Peripheral-Wall Water Vortex Tubes. United Aircraft Research Laboratories Report F-910091-14, prepared under Contract NASw-847, September 1967. Also issued as NASA CR-1028.

24. Kendall, J. S.: Experimental Investigation of Heavy-Gas Containment in Constant-Temperature Radial-Inflow Vortexes. United Aircraft Research Laboratories Report F-910091-15, prepared under Contract NASw-847, September 1967. Also issued as NASA CR-1029.

25. Krascella, N. L.: Spectral Absorption Coefficients of Helium and Neon Buffer Gases and Nitric Oxide-Oxygen Seed Gas Mixture. United Aircraft Research Laboratories Report K-910904-2, prepared under Contract SNPC-70, September 1971.

26. Kinney, R. B.: Theoretical Effect of Seed Opacity and Turbulence on Temperature Distributions in the Propellant Region of a Vortex-Stabilized Gaseous Nuclear Rocket. United Aircraft Research Laboratories Report E-910092-8, prepared under Contract NASw-847, September 1966. Also issued as NASA CR-694.

27. Clark, J. W., B. V. Johnson, J. S. Kendall, A. E. Mensing, and A. Travers: Open-Cycle and Light-Bulb Types of Vortex-Stabilized Gaseous Nuclear Rockets. J. Spacecraft Rockets, vol. 5, no. 8, August 1968, pp. 941-947.

28. Kendall, J. S., W. C. Roman, and P. G. Vogt: Initial Radio-Frequency Gas Heating Experiments to Simulate the Thermal Environment in a Nuclear Light Bulb Reactor. United Aircraft Research Laboratories Report G-910091-17, prepared under Contract NASw-847, September 1968. Also issued as NASA CR-1311.

REFERENCES (Concluded)

29. Kendall, J. S., A. E. Mensing, and B. V. Johnson: Containment Experiments in Vortex Tubes with Radial Outflow and Large Superimposed Axial Flows. United Aircraft Research Laboratories Report F-910091-12, prepared under Contract NASw-847, May 1967. Also issued as NASA CR-993.

30. Douglas, F. C. and R. M. Gagosz: Experimental Investigation of Thermal Annealing of Nuclear-Reactor-Induced Coloration in Fused Silica. United Aircraft Research Laboratories Report D-910082-7, prepared under Contract NASw-768, March 1965. Also issued as NASA CR-304, September 1965.

31. Palma, G. E. and R. M. Gagosz: Optical Absorption in Transparent Materials During 1.5-MeV Electron Irradiation. United Aircraft Research Laboratories Report J-990929-1, prepared under Contract SNPC-70, October 1970.

32. McLafferty, G. H.: Studies of Coolant Requirements for the Transparent Walls of a Nuclear Light Bulb Engine. United Aircraft Research Laboratories Report F-110224-6, March 1967.

33. Tipton, C. R., ed.: Reactor Handbook --- Vol. I - Materials. Interscience Publishers, Inc., New York, New York, 1960.

34. Dmitrievskii, V. A. and A. L. Migachev: Dissociation of the UF_6 Molecule Under the Action of Fragments from Fission of the Uranium Nucleus. Atomnaya Energiya, vol. 6, no. 5, 1959.

35. Nesmeyanov, A. N.: Vapor Pressure of the Chemical Elements. Elsevier Publishing Company, Amsterdam, 1963.

LIST OF SYMBOLS

A_F	Fuel injection control valve area, cm^2
A_p	Propellant channel cross-sectional flow area, m^2
A_{TW}	Area of transparent wall, cm^2
a_ω	Spectral absorption coefficient, cm^{-1}
d_e	Effective diameter, m
dT/dr	Radial temperature gradient, $^oK/cm$
E	Energy, MeV
H_p	Propellant enthalpy, J/kg
K_F	Fuel injection flow rate calibration factor, $g/sec\text{-}cm^2$
P	Pressure, atm
P_F	Fuel partial pressure, atm
P_I	Fuel injection pressure, atm
P_N	Neon partial pressure, atm
P_S	Seed partial pressure, atm
P_T	Total engine pressure, atm
Pr	Prandtl number, dimensionless
Q	Engine power, MW
Q_{COND}	Energy conducted in buffer region, MW/cell
Q_{CONV}	Energy convected by buffer gas, MW/cell
Q'''_{CONV}	Volumetric convective energy in buffer region, MW/cm^3 per cell
Q_{EX}	Excess absorbed energy in buffer region, MW/cell

LIST OF SYMBOLS (Continued)

Q_{EX}^{III}	Volumetric net absorbed energy in buffer region, MW/cm^3 per cell
Q_{FP}	Fission product power, MW
Q_{IND}^{TW}	Induced absorption in transparent wall, MW
Q_{UV}	Transparent-wall uv heat load, MW
Q_{UV}^{TW}	UV radiation absorption in transparent wall, MW
Q_{WP}	Convective heat flux to the walls, MW/m^2
q	Heat flux at edge-of-fuel location, erg/cm^2-sec
q_{ω}	Spectral heat flux, erg/cm-sec
q_{ω}^{bb}	Black-body spectral heat flux, erg/cm-sec
R	Radius, cm
R_{AF}	Radial location of onset of axial buffer flow, cm
R_C	Cavity radius, m
R_{EOF}	Edge-of-fuel location, cm
R_{STAG}	Stagnation surface location, cm
R_{TW}	Inner radial boundary of transparent wall, m
R_1	Inner radial boundary of region of analysis, cm
R_2	Radius of fuel region, cm
R_3	Inner radial boundary of transparent wall, cm
r	Radius, m
Re	Reynolds number, dimensionless

LIST OF SYMBOLS (Continued)

Ri	Richardson number, dimensionless
St	Stanton number, dimensionless
T	Temperature, ^{o}K or ^{o}R
T*	Effective black-body fuel radiating temperature, ^{o}K or ^{o}R
T_{TW}	Buffer-gas temperature at transparent wall, ^{o}K or ^{o}R
T_W	Specimen temperature, ^{o}K
T_{ω}^{bb}	Effective spectral black-body radiating temperature, ^{o}K or ^{o}R
t	Time, sec
t_{op}	Operating time, sec
V	Element of volume, cm^3
V_Z	Axial velocity in buffer region, cm/sec
V_{ϕ_1}	Average tangential velocity at transparent peripheral wall, m/sec
W_B	Total buffer weight flow, kg/sec
W_{BR}	Radial buffer weight flow, kg/sec
W_F	Fuel injection rate, g/sec
W_p	Propellant mass flow rate, kg/sec
α	Absorption coefficient, cm^{-1}
$\alpha(\dot{D})$	Induced absorption coefficient, cm^{-1}
α_I	Nuclear-radiation-induced absorption coefficient for reference engine, cm^{-1}
$\Delta Q/Q_o$	Power level change

LIST OF SYMBOLS (Continued)

ΔR	Distance from edge-of-fuel location, cm
ΔR_{TW}	Transparent-wall thickness, cm
Δr_{EFF}	Effective thickness of transparent-wall material, cm
$\Delta \overline{T}_B$	Buffer mixed-mean temperature rise, ^{o}K
$\Delta \omega$	Wave-number-group width, cm^{-1}
δA_{F_1}	Imposed change in fuel-injection control valve area, cm^2
$\partial V_Z/\partial r$	Axial shear (i.e., local radial gradient of axial velocity), m/sec/m
$\partial \rho/\partial r$	Local radial gradient of total density, $kg/m^3/m$
λ	Wavelength of photon, μ
μ	Hydrogen propellant viscosity, $N \cdot sec/m^2$
ρ	Density, g/cm^3
τ_C	Fuel circulation time, sec
τ_ω	Optical depth, dimensionless
ω	Wave number, cm^{-1}

Subscripts

i	i^{th} region or interval
o	Denotes reference condition

TABLE I

DISTRIBUTION OF FISSION ENERGY RELEASE
IN NUCLEAR LIGHT BULB REFERENCE ENGINE

Engine Power = 4600 MW
Fuel - U-233
See Figs. 3 and 4 for Energetics of
Fission and Fission Product Decay Heating Rate

Energy Source	Power Created from Each Source, MW			
	Operating Time, t_{op} - sec			
	10	100	1000	10,000
Fission Fragments	4253.3	4192.4	4130.7	4104.1
Neutrons	124.7	122.6	120.8	119.9
Prompt Gamma Rays	183.0	180.0	177.5	176.0
Delayed Gamma Rays	7.4	30.4	55.0	77.0
Beta Particles	31.6	74.6	116.0	123.0

TABLE II

DISTRIBUTION OF FISSION ENERGY DEPOSITION
IN NUCLEAR LIGHT BULB REFERENCE ENGINE

Engine Power = 4600 MW
Engine Operating Time = 1000 sec
Nuclear Fuel Residence Time in Active Core = 4.0 sec
See Table I for Distribution of Fission Energy Release

Energy Source	Fission Fragment Separation	Rate of Fission Energy Deposition, MW				
		Principal Component				
		Fuel and Buffer Gases	Hydrogen Propellant	Structure	Leakage	Separator
(a) Fuel Circulation Time, τ_c = 16 sec						
Fission Fragments	No	4115.0	--	--	--	15.7
	Yes	4115.0	--	--	--	15.7
Neutrons	No	--	50.6	62.8	7.3	0.1
	Yes	--	50.6	62.8	7.3	0.1
Prompt Gamma Rays	No	1.6	1.7	154.7	19.2	0.3
	Yes	1.6	1.7	154.7	19.2	0.3
Delayed Gamma Rays	No	0.4	0.8	48.5	3.4	1.9
	Yes	0.4	0.8	48.0	3.4	2.4
Beta Particles	No	58.8	3.3	3.3	--	50.6
	Yes	43.8	2.5	2.4	--	67.3
(b) Fuel Circulation Time, τ_c = 40 sec						
Fission Fragments	No	4101.6	--	--	--	29.1
	Yes	4101.6	--	--	--	29.1
Neutrons	No	--	50.4	63.0	7.3	0.1
	Yes	--	50.4	63.0	7.3	0.1
Prompt Gamma Rays	No	1.6	1.7	154.7	19.2	0.3
	Yes	1.6	1.7	154.7	19.2	0.3
Delayed Gamma Rays	No	0.4	0.8	48.2	3.4	2.2
	Yes	0.4	0.8	48.0	3.4	2.4
Beta Particles	No	50.0	2.7	2.8	--	60.5
	Yes	43.8	2.5	2.4	--	67.3

(Continued)

TABLE II (Concluded)

Energy Source	Fission Fragment Separation	Rate of Fission Energy Deposition, MW — Principal Component: Fuel and Buffer Gases	Hydrogen Propellant	Structure	Leakage	Separator
(c) Fuel Circulation Time, τ_c = 80 sec						
Fission Fragments	No	4079.2	--	--	--	51.5
	Yes	4079.2	--	--	--	51.5
Neutrons	No	--	50.2	63.2	7.3	0.1
	Yes	--	50.6	63.2	7.3	0.1
Prompt Gamma Rays	No	1.6	1.7	154.7	19.2	0.3
	Yes	1.6	1.7	154.7	19.2	0.3
Delayed Gamma Rays	No	0.4	0.8	47.1	3.4	3.3
	Yes	0.4	0.8	48.0	3.4	2.4
Beta Particles	No	46.8	2.6	2.6	--	64.0
	Yes	43.8	2.5	2.4	--	67.3

TABLE III

NEUTRON AND GAMMA HEATING

Engine Power = 4600 MW
Engine Operating Time = 1000 sec
Nuclear Fuel Residence Time in Active Core = 4.0 sec
Fuel Circulation Time = 16.0 sec
See Ref. 2 for Description of Materials in Engine Components

Component	Neutron and Prompt Gamma Heating Rate, MW	Delayed Gamma Heating Rate, MW		Total Neutron and Gamma Heating Rate, MW	
		No Fission Fragment Separation	Total Fission Fragment Separation	No Fission Fragment Separation	Total Fission Fragment Separation
Pressure Vessel	15.5	3.3	3.3	18.8	18.8
Upper End Graphite	2.4	0.5	0.5	2.9	2.9
Upper End BeO	18.8	4.0	4.0	22.8	22.8
Lower End Graphite	15.2	3.3	3.2	18.5	18.4
Lower End BeO	26.0	5.6	5.5	31.6	31.5
Axial BeO	79.8	17.3	17.1	97.1	96.9
Axial Graphite	43.2	9.3	9.2	52.5	52.4
Transparent Wall	9.4	2.0	2.0	11.4	11.4
Cavity Liner	4.0	0.9	0.9	4.9	4.9
Fuel Cycle	0.9	0.2	0.2	1.1	1.1
Tie Rods	4.7	1.0	1.0	5.7	5.7
Flow Divider	6.4	1.4	1.4	7.8	7.8
Nozzles	0.1	0.1	0.1	0.2	0.2
Heat Exchanger Region	0.4	1.9	2.4	2.3	2.8
Direct Hydrogen Heating	52.3	0.8	0.8	53.1	53.1
Leakage	19.2	3.4	3.4	22.6	22.6
Total	298.3	55.0	55.0	353.3	353.3

TABLE IV

SUMMARY OF NEON BUFFER-GAS HEAT TRANSFER AND FLOW REQUIREMENTS FOR DIFFERENT SILICON SEED PARTIAL PRESSURES IN BUFFER-GAS AND EDGE-OF-FUEL REGIONS

Reference Engine Power Level = 4600 MW

See Fig. 5 for Geometry and Dimensions of Region of Analysis

See Fig. 6 for Fuel, Seed, and Neon Radial Partial Pressure Distributions in Region of Analysis

Stagnation Surface 0.30 cm Inside Edge-of-Fuel Location

	Silicon Seed Partial Pressure, atm		
	10.0	1.0	0.1
Neon Inlet Temperature, °K	1110	1110	1110
Energy Conducted into Buffer Gas, MW/cell	0.64	0.64	0.64
Thermal Radiation Absorbed, MW/cell	2.93	4.19	29.26
Total Energy Convected, MW/cell	3.57	4.83	29.90
Total Neon Weight Flow per Cell, kg/sec	12.4	17.6	119.0
Neon Mixed-Mean Temperature Rise, °K	284.0	266.0	244.0
Average Neon Axial Velocity, m/sec	2.19	3.04	21.37
Axial Dynamic Pressure, atm	0.0024	0.0049	0.23

TABLE V

SUMMARY OF ENERGY DEPOSITION RATES IN TRANSPARENT WALLS OF NUCLEAR LIGHT BULB ENGINE

Wall Thickness = 0.0127 cm
Values Shown are Totals for Seven Cavities

Ultraviolet Radiation Absorption ($T = 1073^{\circ}K$)	1.9 MW
Thermal Radiation Absorption Due to Nuclear-Radiation-Induced Absorption Coefficient ($\alpha_I = 0.1\ cm^{-1}$)	1.1 MW
Nuclear Radiation Energy Absorption	
Neutrons	1.1 MW
Gamma Rays	10.3 MW
Beta Particles	3.3 MW
Thermal Conduction from Buffer Gas	--
Convection From Propellant Stream	
No Film or Transpiration Cooling	110.0 MW
Film or Transpiration Cooling to Reduce Stanton Number by Factor of 3	36.7 MW*
Total Energy Deposition Rate	
No Film or Transpiration Cooling on Propellant Stream Side	127.7 MW
Film or Transpiration Cooling to Reduce Stanton Number by Factor of 3 on Propellant Stream Side	54.4 MW*

*Reference Engine Heat Loads.

TABLE VI

SUMMARY OF THERMAL RADIATION HEAT LOADS
ON END WALLS, TRANSPARENT WALLS,
AND PROPELLANT CHANNEL LINERS

Values Shown are Totals for Seven Cavities

Component	Mode of Heat Transfer	Heat Load, MW
Transparent Walls	Ultraviolet Radiation Absorption	1.9
	Thermal Radiation Absorption Due to Nuclear Radiation Induced Absorption Coefficient	1.1
Cavity End Walls	Thermal Radiation, View Factor = 1.0, Reflectivity = 0.6 (Tungsten)	390
	Thermal Radiation, View Factor = 0.5, Reflectivity = 0.6 (Tungsten)	195*
Propellant Channel Liners	Thermal Radiation, Reflectivity = 0.9 (Aluminum)	100

*Reference Engine Heat Load.

TABLE VII

SUMMARY OF CONVECTION HEAT LOADS ON
TRANSPARENT WALLS AND PROPELLANT CHANNEL LINERS

Values Shown are Totals for Seven Cavities

Propellant Channel Liner Area = 27.4 m^2

Support Strut Area = 7.33 m^2

Transparent-Wall Area = 19.5 m^2

Component	Mode of Heat Transfer	Heat Load, MW	
		No Cooling	Cooling to Reduce Stanton Number By Factor of 3*
Transparent Walls	Convection From Propellant Stream	110.0	36.7
Propellant Channel Liners	Convection From Propellant Stream	205.0	68.3

*Film cooling, transpiration cooling, or selective seeding of propellant.

TABLE VIII

FULL-POWER, STEADY-STATE MODERATOR AND STRUCTURE HEAT DEPOSITION RATES

Fuel - U-233

Region	Mechanism of Heating	Reference Engine Heat Deposition Rate, MW (Ref. 1)	Modification I Heat Deposition Rate, MW (Ref. 7)	Modification II Heat Deposition Rate, MW (Present Report)
Pressure Vessel	Neutron and Gamma	11.55*	11.55	12.5
Nozzles	Neutron and Gamma	0.08	0.08	0.2
Flow Divider	Neutron and Gamma and Conduction	7.15	7.15	7.8
Tie Rods	Neutron and Gamma and Conduction	5.39	5.39	5.7
Cavity End Walls	Thermal Radiation and Conduction	6.40	73.0	195.1
Propellant Chanel Liners	Thermal Radiation and Conduction	81.0	112.0	173.0
Transparent Structure	Thermal Radiation, Convection, Neutron, Gamma, and Beta	119.0	65.5	54.4
Neon and Fuel Circuit	Removal of Heat From Fuel	64.0	70.7	159.0
Upper and Lower End Moderators	Neutron and Gamma	70.0	70.0	75.8
Beryllium Oxide Moderator	Neutron and Gamma	89.5	89.5	96.9
Graphite Moderator	Neutron and Gamma	48.6	48.6	52.3
Direct Hydrogen Heating	Neutron, Gamma, and Beta	58.9	58.0	56.6
TOTAL		561.57	612.37	889.3
PERCENT OF TOTAL POWER		12.2	13.3	19.3

*Total heating in pressure vessel is 18.8 MW. It is assumed that only 2/3 of the total will be removed by the closed secondary hydrogen coolant circuit and the remaining 1/3 will be removed by the hydrogen which is used for transpiration cooling of the exhaust nozzles.

TABLE IX

FULL-POWER, STEADY-STATE TEMPERATURE AND ENTHALPY IN SECONDARY HYDROGEN CIRCUIT

Hydrogen Coolant Circuit Flow = 19.3 kg/sec

See Fig. 2 for Flow Diagram

Location	Temperature, ^{o}K	Enthalpy, J/g
Primary Hydrogen H_2-H_2 Heat Exchanger Outlet	90	1010
Pump Outlet	92	1020
Pressure Vessel Liner Outlet	138	1695
Tie Rod, Flow Divider, and Propellant Channel Liner Outlet	802	11,415
Transparent Wall Outlet	985	14,180
Space Radiator H_2-H_2 Heat Exchanger Outlet	573	8110

TABLE X

SUMMARY OF ENERGY DEPOSITION RATES, TEMPERATURES, AND FLOW CONDITIONS IN FUEL AND NEON CIRCUIT

Fuel Region (volume inside edge-of-fuel radius):-

- Fuel Weight Flow = 3.5 kg/sec
- Fuel Inlet Temperature = 1500°K
- Average Fuel Temperature Rise = 23,900°K
- Net Energy Deposition Rate in Fuel = 34.9 MW
- Neon Weight Flow in Fuel Region = 1.44 kg/sec
- Neon Inlet Temperature = 6440°K
- Average Neon Temperature Rise = 10,060°K
- Net Energy Deposition Rate = 15.4 MW

Buffer-Gas Region (volume between edge of fuel and transparent wall):-

- Neon Axial Bypass Weight Flow = 74.5 kg/sec
- Neon Axial Bypass Inlet Temperature = 610°K
- Net Energy Deposition Rate
  - Beta Particle Energy = 5.9 MW
  - Gamma Ray Energy = 0.5 MW
  - Total = 6.4 MW
- Average Neon Axial Bypass Flow Temperature Rise = 80°K
- Neon Cavity Buffer Flow = 12.4 kg/sec
- Neon Cavity Flow Inlet Temperature = 610°K
- Net Energy Deposition Rates
  - Conduction From Fuel Region = 4.5 MW
  - Thermal Radiation Absorption = 20.5 MW
  - Beta Particle Energy = 7.8 MW
  - Gamma Ray Energy = 0.7 MW
  - Total = 33.5 MW
- Average Neon Cavity Buffer Flow Temperature Rise = 2580°K

Thru-Flow Ports:-

- Fuel and Neon Mixed-Mean Inlet Temperature = 6070°K
- Mixture Residence Time in Thru-Flow Duct = 0.01 sec
- Energy Deposition By Fission Fragments = 9.0 MW
- Neon Axial Bypass Flow Rate = 74.5 kg/sec
- Neon Axial Bypass Flow Inlet Temperature = 690°K
- Neon Manifold Bypass Flow Rate = 12.0 kg/sec
- Neon Manifold Bypass Flow Inlet Temperature = 610°K

(Continued)

TABLE X (Concluded)

Fuel-Neon Vortex Separator:- Fuel-Neon Mixed-Mean Inlet Temperature = 1500°K Mixture Residence Time in Separator = 0.10 sec Fuel Outlet Temperature = 1500°K Fuel Flow Rate = 3.5 kg/sec Neon Outlet Temperature = 1500°K Neon Flow Rate = 98.7 kg/sec
Neon/Primary-Hydrogen Heat Exchanger:- Neon Inlet Temperature = 1500°K Neon Flow Rate = 98.7 kg/sec H_2 Inlet Temperature = 540°K H_2 Flow Rate = 19.2 kg/sec Neon Outlet Temperature = 610°K H_2 Outlet Temperature = 852°K
Liquid Uranium Crucible:- Net Energy Deposition Rates Beta Particle Energy = 50.6 MW Gamma Ray Energy = 2.2 MW Fission Fragment Energy = 6.7 MW Total = 59.5 MW Nuclear Fuel Residence Time = 12.0 sec H_2 Flow Rate = 19.3 kg/sec H_2 Inlet Temperature = 866°K H_2 Outlet Temperature = 1064°K

TABLE XI

FULL-POWER, STEADY-STATE TEMPERATURE AND ENTHALPY LEVELS IN NEON AND FUEL CIRCUIT

Total Neon Flow Per Cavity* = 14.1 kg/sec (98.7 kg/sec for 7 cavities)
Total Fuel Flow Per Cavity = 0.5 kg/sec (3.5 kg/sec for 7 cavities)

Location	Temperature, °K	Enthalpy, J/g
H_2-Ne Heat Exchanger Outlet	610	640
Pump Outlet*	613	645
Cavity Outlet	6070	6440
H_2-Ne Exchanger Inlet	1500	1585

*The total required neon flow rate is 14.1 kg/sec for each cavity (98.7 kg/sec for 7 cavities). 12.4 kg/sec flows into each cavity (86.7 kg/sec for 7 cavities) of which 1.75 kg/sec exits through the thru-flow ports and 10.65 kg/sec exits through axial bypass ports in the end walls (12.2 kg/sec and 74.5 kg/sec, respectively, for 7 cavities). The axial bypass flow and the remaining 1.7 kg/sec (12.0 kg/sec for 7 cavities) is mixed with the flow which exits from the cavity to condense the fuel before the neon fuel mixture enters the separator.

TABLE XII

FULL-POWER, STEADY-STATE TEMPERATURE AND ENTHALPY LEVELS IN PRIMARY HYDROGEN PROPELLANT CIRCUIT

See Fig. 2 for Flow Diagram
Hydrogen Propellant Flow = 19.3 kg/sec
See Text for Discussion of Cooling Sequence Options

Location	Temperature, °K	Enthalpy, J/g
Pump Inlet	20	280
Pump Outlet	58	680
Secondary Heat Exchanger Outlet	540	7780
Fuel Cycle Heat Exchanger Outlet	852	12,590
Fuel-Neon Separator Outlet	1064	15,700
Turbine Outlet	946	13,900
Upper End Moderator Outlet	1016	15,240
Axial Beryllium Oxide Outlet	1354	20,290
Lower End Moderator Outlet	1518	22,910
Lower End-Wall Liner Outlet	1814	27,990
Axial Graphite Outlet	1968	30,720
Upper End-Wall Liner Outlet	2264	35,880
Propellant, Including Direct H_2 Heating	6670	240,500

TABLE XIII

SUMMARY OF REFERENCE ENGINE DESIGN CHARACTERISTICS
WITH REVISED COOLING SEQUENCE

Cavity Configuration	Seven separate, 1.83-m-long cavities having a total volume of 4.82 m^3
Cavity Pressure	500 atm
Specific Impulse	1870 Sec
Total Propellant Flow (including seed and nozzle transpiration coolant flow)	22.4 kg/sec
Thrust	409,000 N
Engine Weight	31,750 kg
Space Radiator Weight	5500 kg
Total System Weight (Engine and Space Radiator)	37,250 kg
Total System Thrust-to-Weight Ratio	1.12

L-910900-16 FIG. 1

SKETCHES ILLUSTRATING PRINCIPLE OF OPERATION OF NUCLEAR LIGHT BULB ENGINE

ENGINE LENGTH = 6.93 M MAX. ENGINE DIAM = 3.90 M

UNIT CAVITY LENGTH = 1.83 M UNIT CAVITY AV DIAM = 0.65 M

(a) OVERALL CONFIGURATION

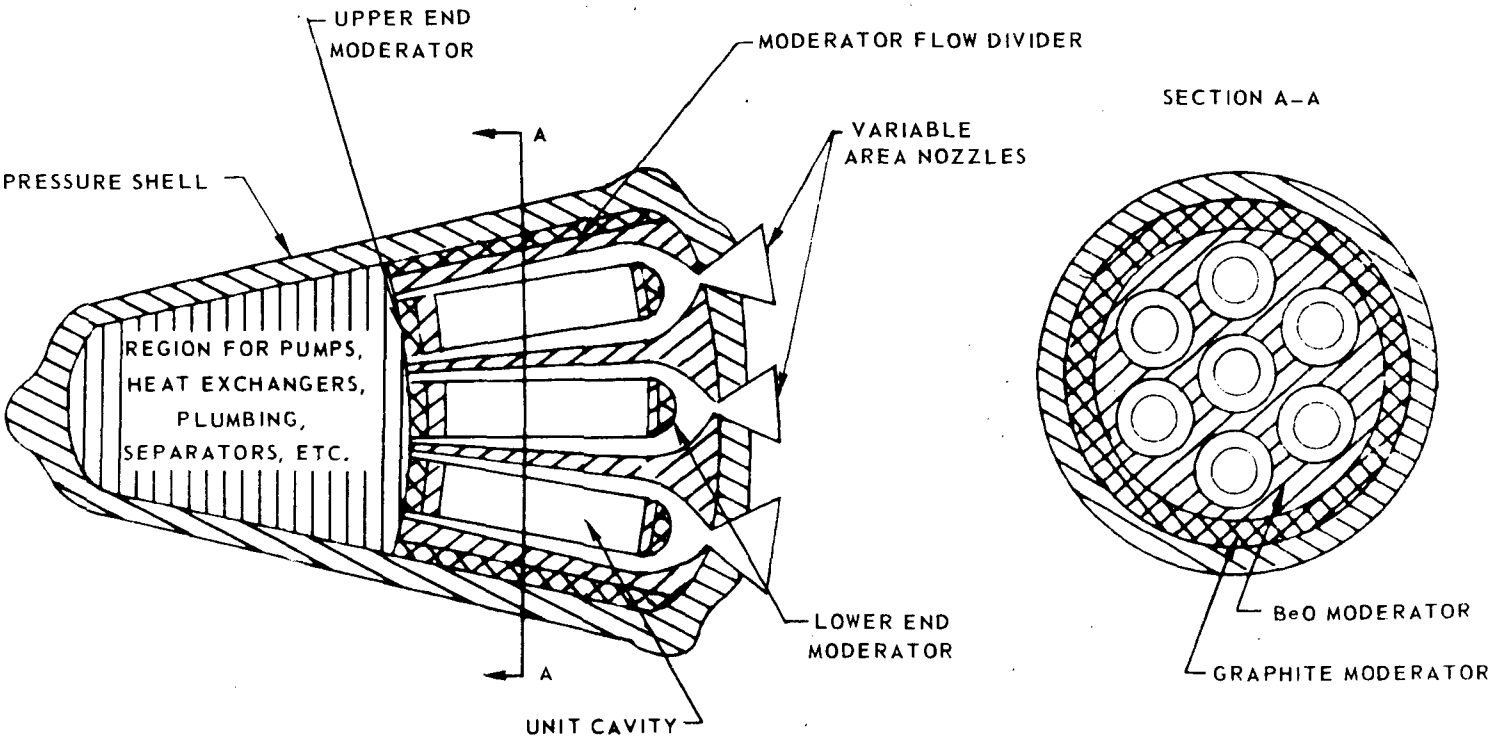

(b) CONFIGURATION OF UNIT CAVITY

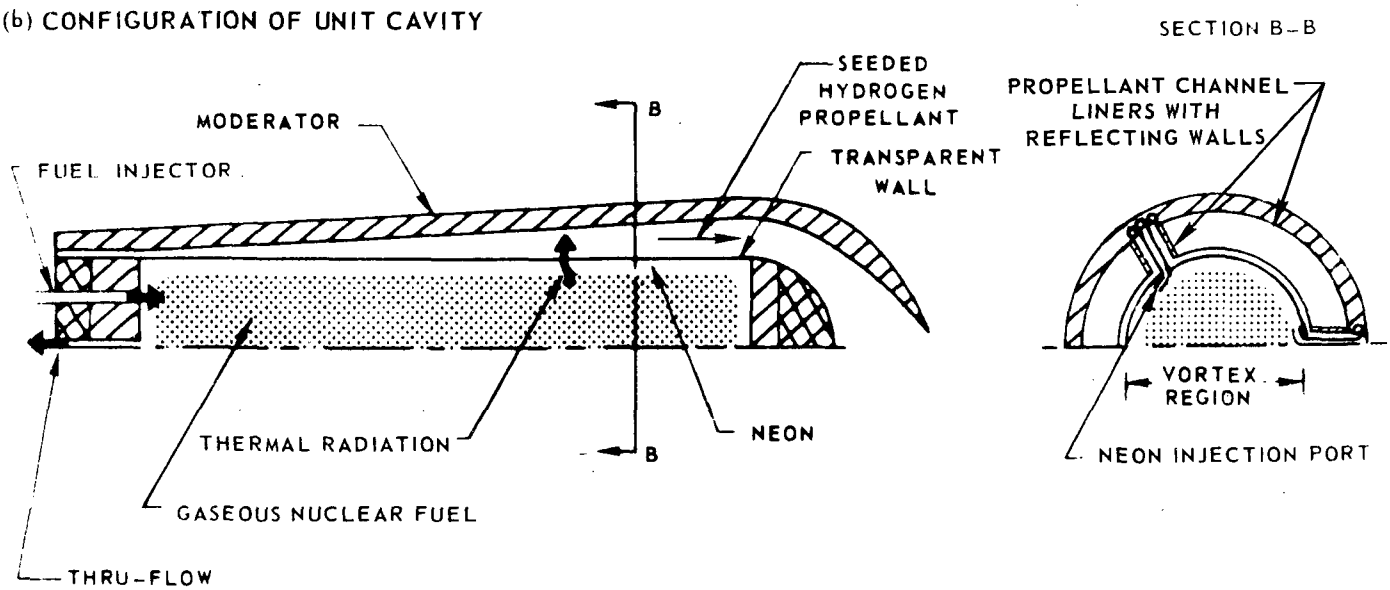

NUCLEAR LIGHT BULB FLOW DIAGRAM

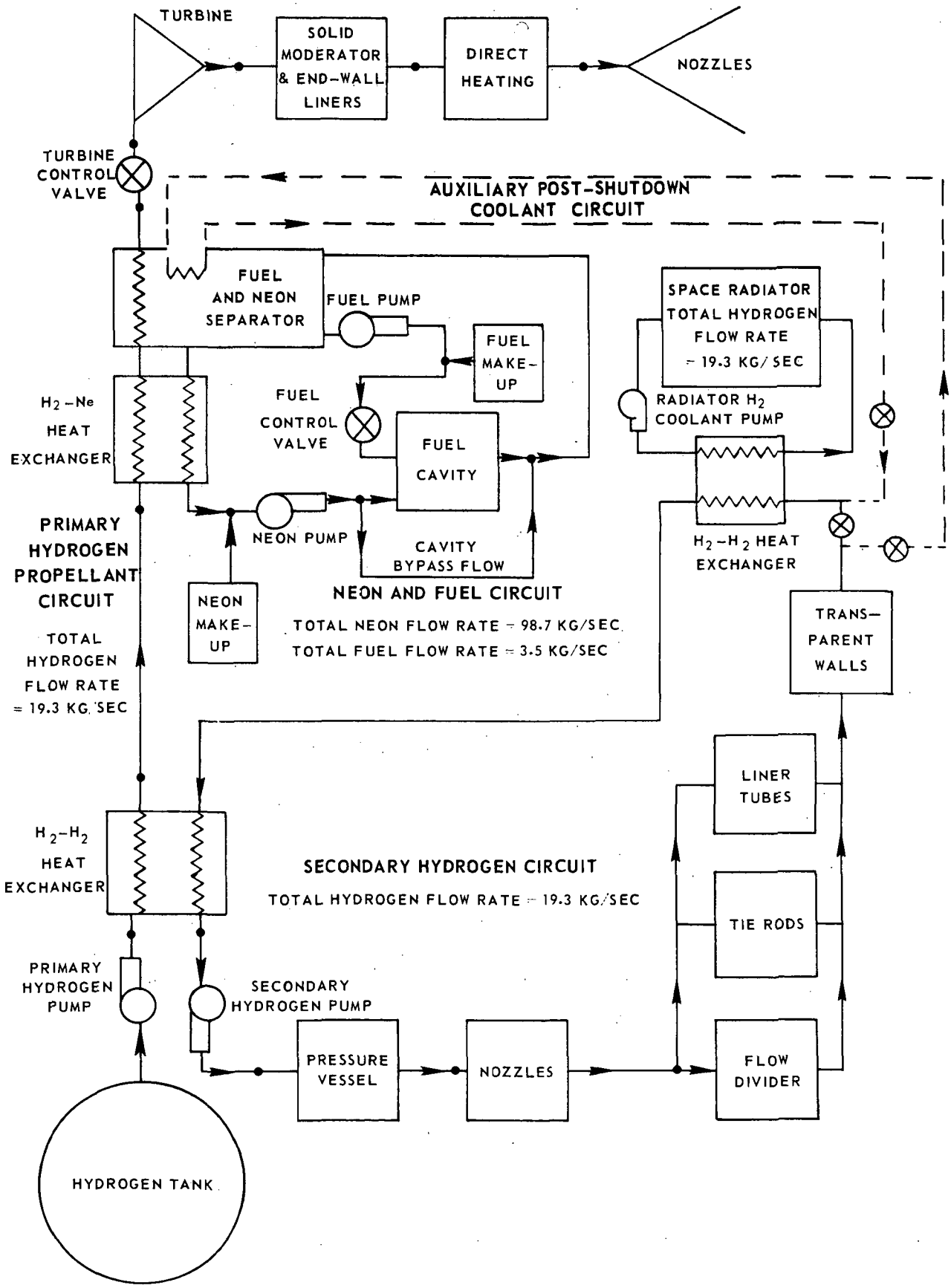

L-910900-16

FIG. 3

ENERGY RELEASED BY NEUTRONS, GAMMA RAYS, BETA PARTICLES, AND FISSION FRAGMENTS AS A FUNCTION OF TIME AFTER FISSION OF U-233

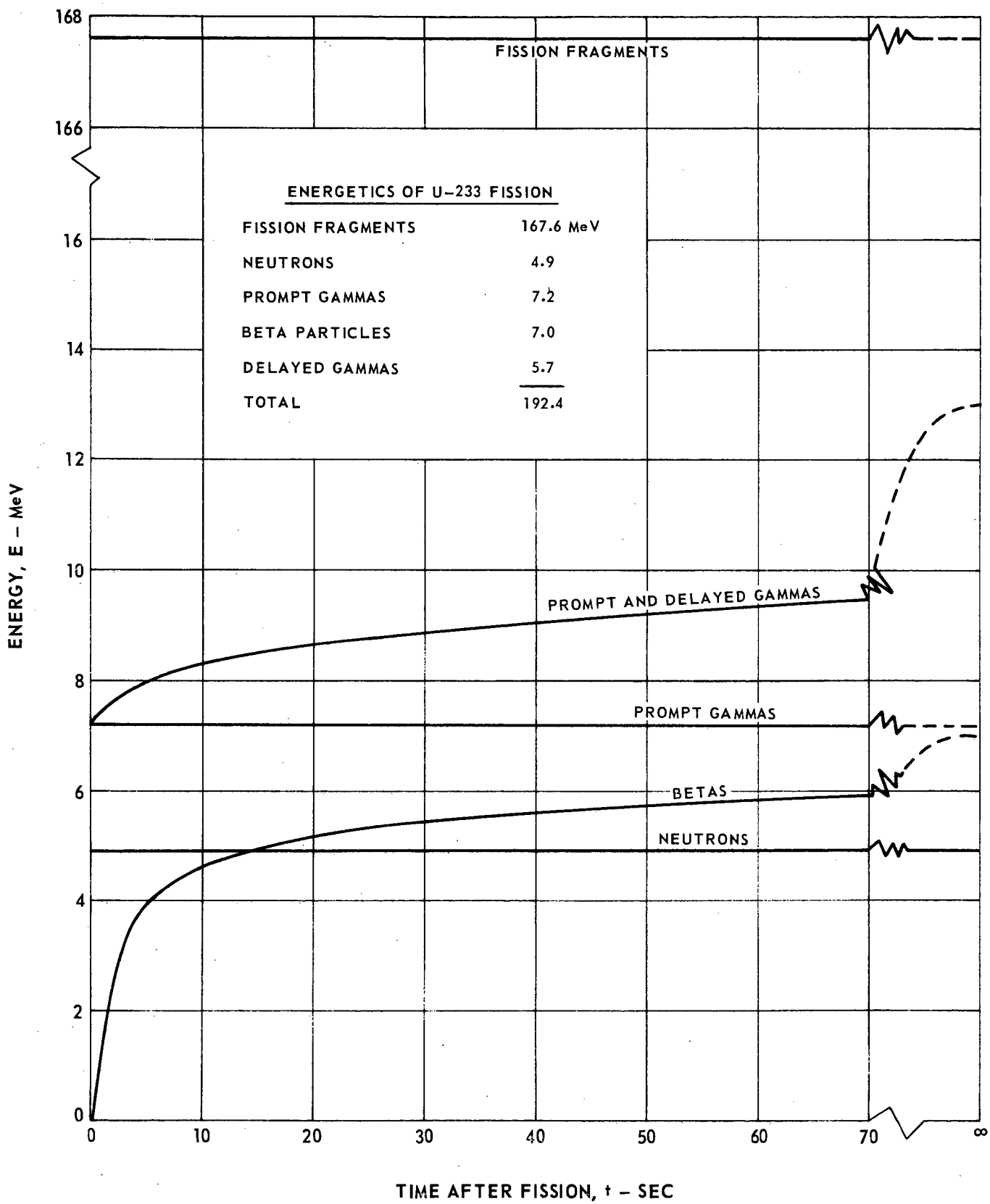

FIG. 4

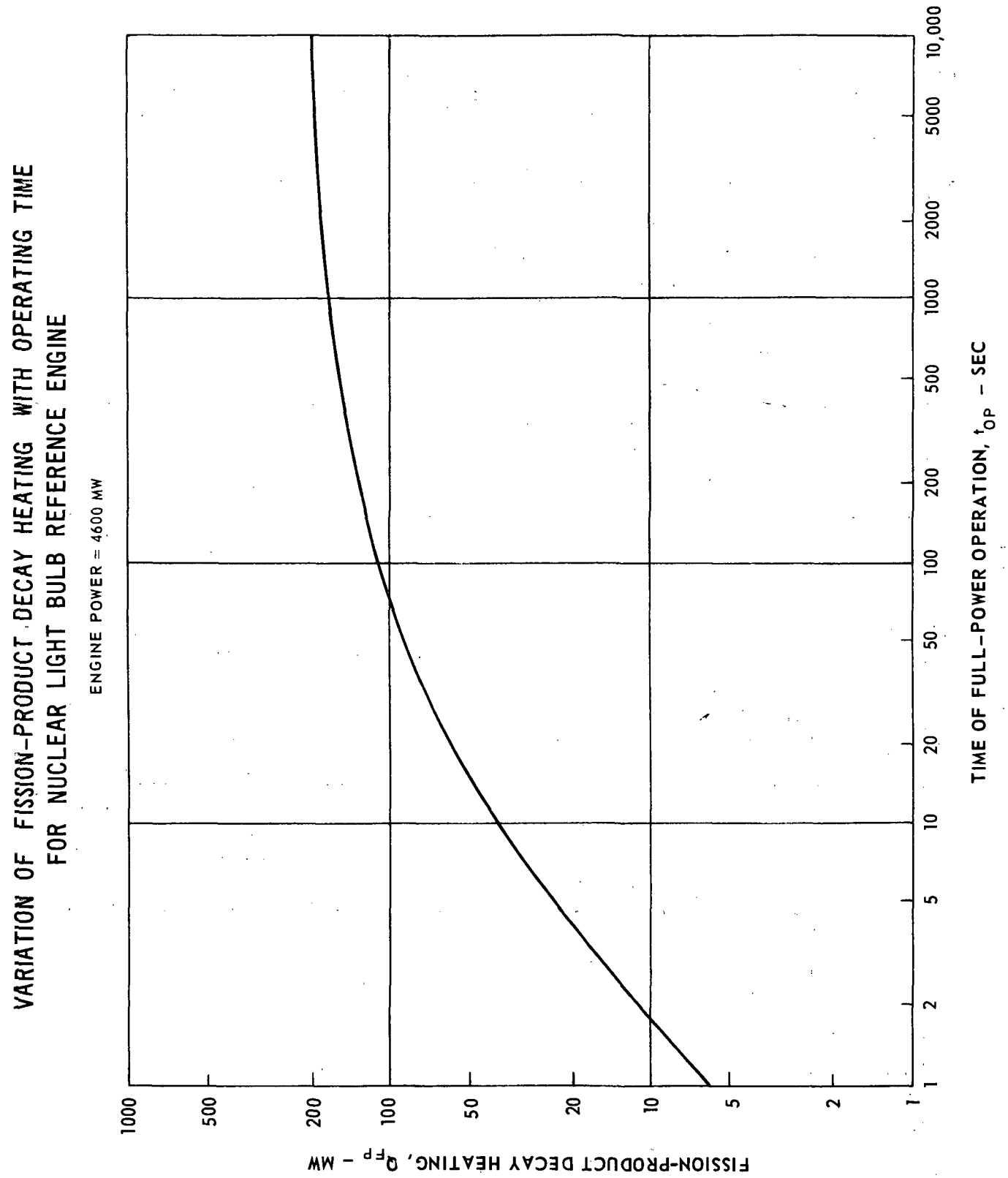
VARIATION OF FISSION-PRODUCT DECAY HEATING WITH OPERATING TIME
FOR NUCLEAR LIGHT BULB REFERENCE ENGINE
ENGINE POWER = 4600 MW
FISSION-PRODUCT DECAY HEATING, Q_{FP} - MW
1000
500
200
100
50
20
10
5
2
1
1
2
5
10
20
50
100
200
500
1000
2000
5000
10,000
TIME OF FULL-POWER OPERATION, t_{OP} - SEC

FIG. 5

BUFFER-GAS FLOW PATTERN ASSUMED IN CONVECTION AND CONDUCTION ANALYSIS FOR THE TEMPERATURE DISTRIBUTIONS IN BUFFER REGION

SEE FIG. 6 FOR FUEL, BUFFER-GAS, AND SEED RADIAL PARTIAL PRESSURE DISTRIBUTIONS IN REGION OF ANALYSIS

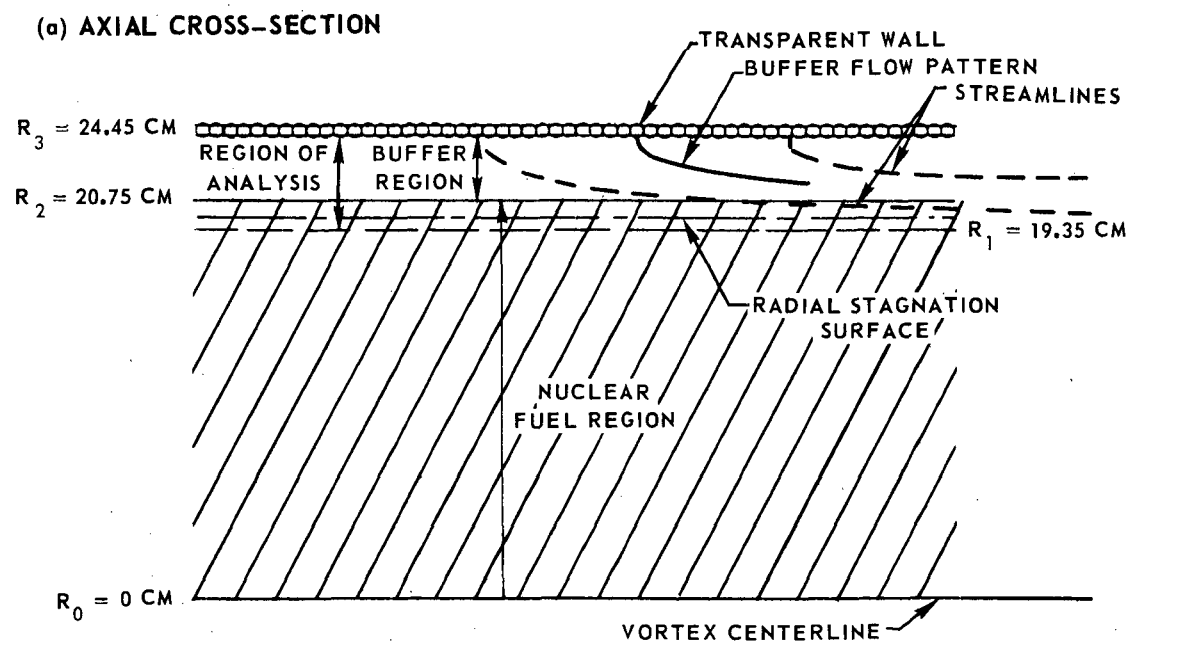

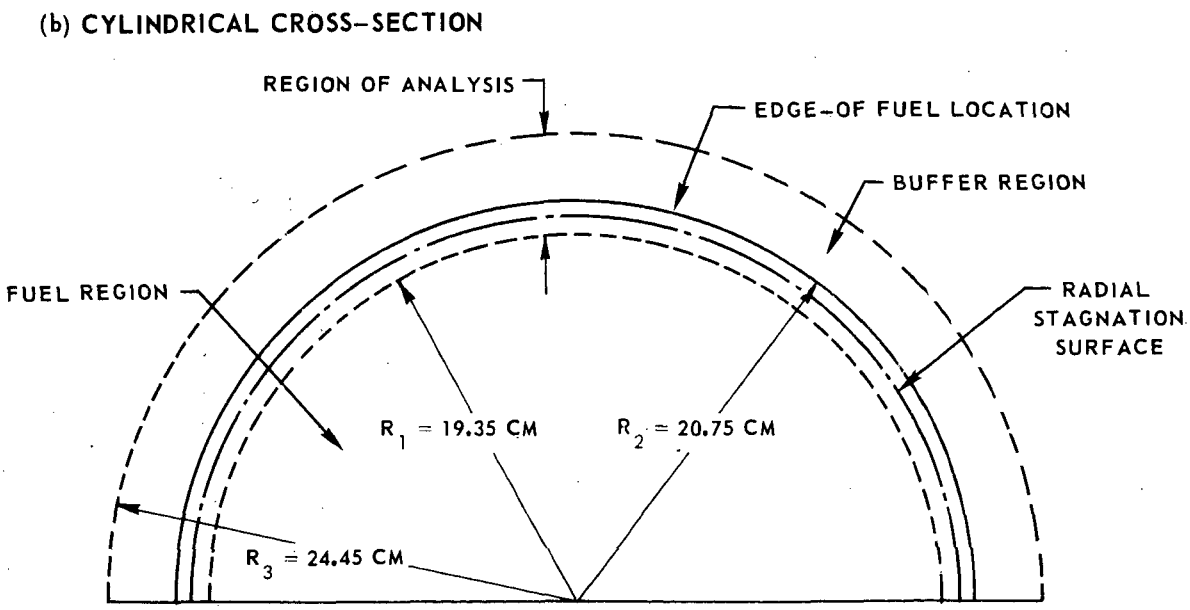

TYPICAL FUEL, SEED, AND NEON RADIAL PARTIAL PRESSURE DISTRIBUTIONS USED FOR RADIANT HEAT TRANSFER CALCULATIONS

$$P_T = P_F + P_N + P_S = 500 \text{ ATM}$$

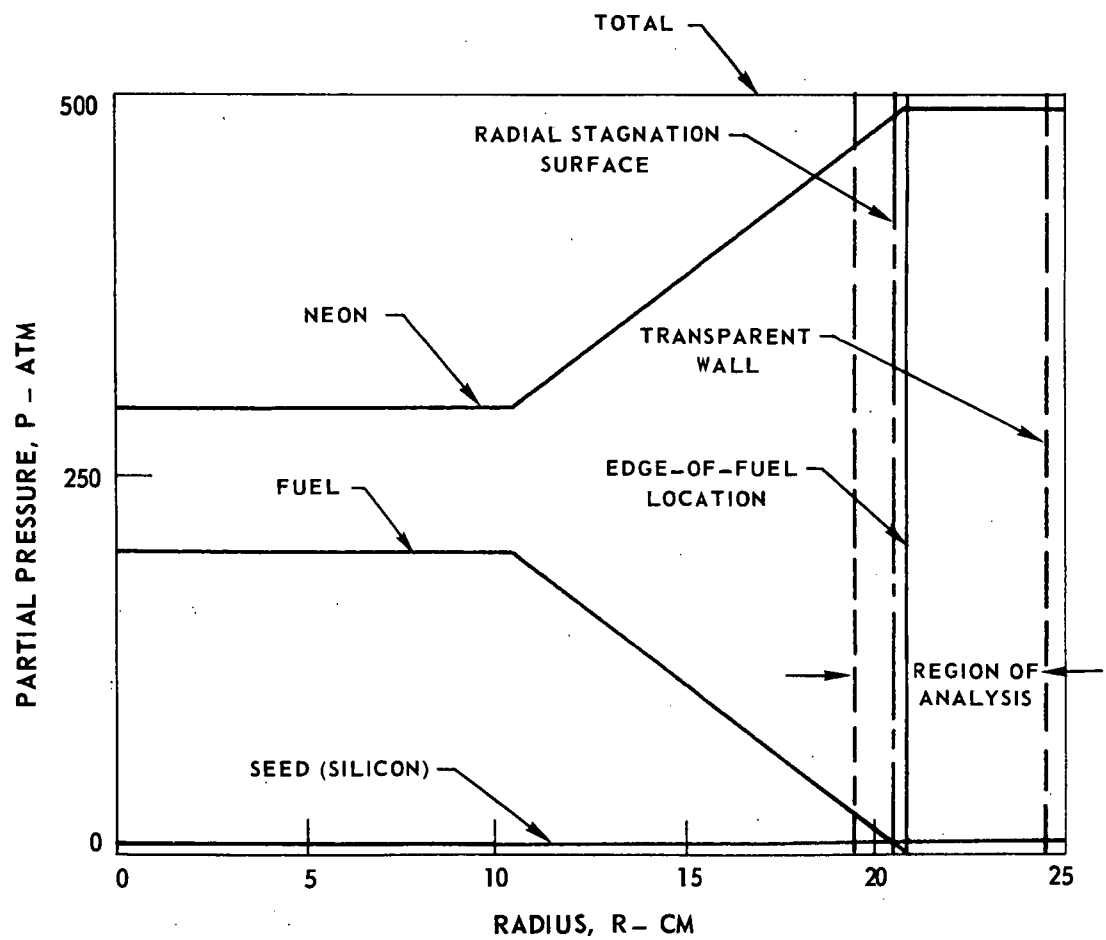

L-910900-16

FIG. 7

VARIATION OF SPECTRAL ABSORPTION COEFFICIENT FOR URANIUM AND SILICON WITH WAVE NUMBER FOR A TEMPERATURE OF 10,000°K

URANIUM PRESSURE = 5 ATM

SILICON PRESSURE = 10 ATM

SPECTRAL ABSORPTION COEFFICIENTS TAKEN FROM REF. 14.

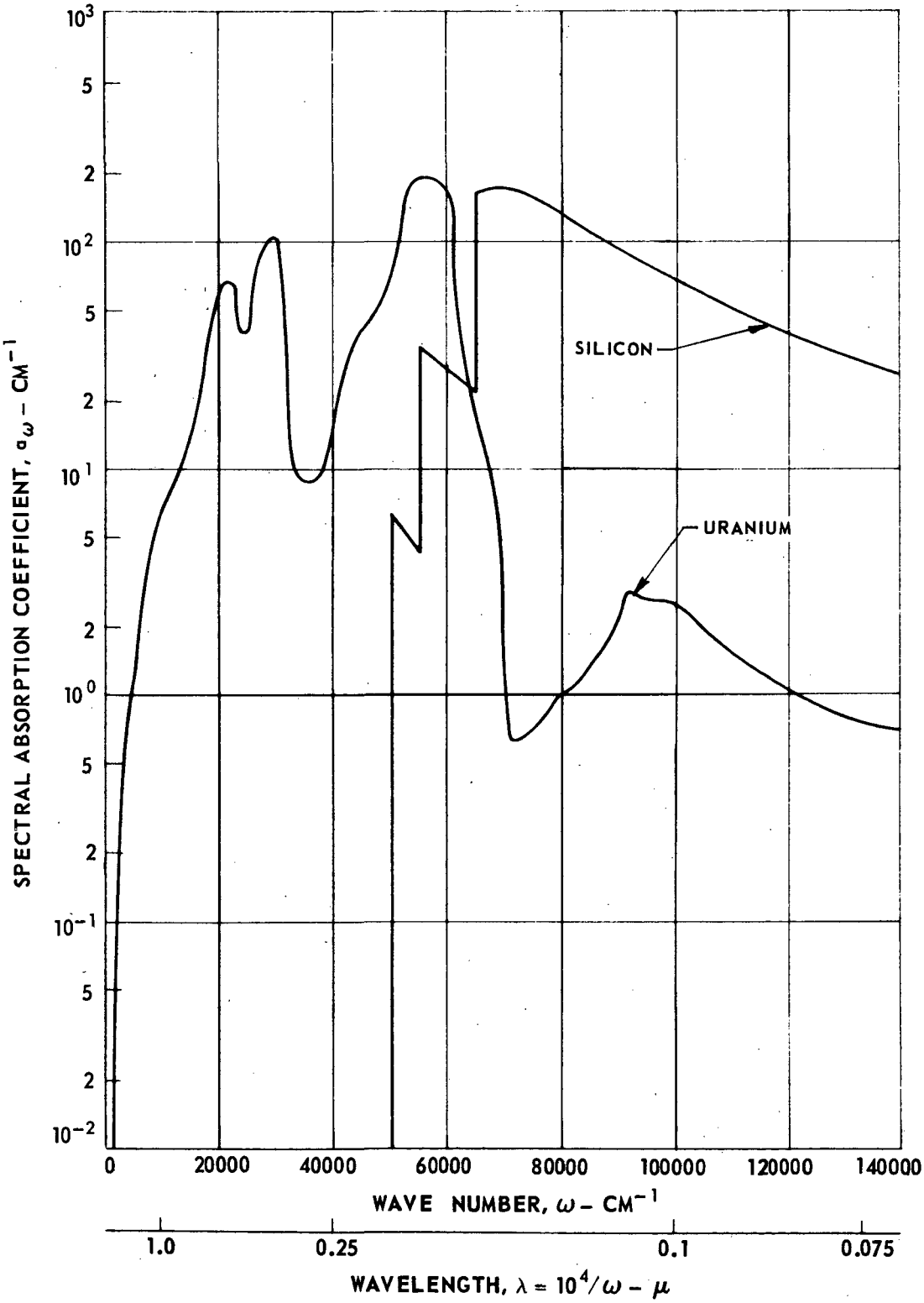

TEMPERATURE DISTRIBUTIONS FOR REFERENCE ENGINE POWER LEVEL FOR VARIOUS SILICON SEED PARTIAL PRESSURES IN EDGE-OF-FUEL AND BUFFER-GAS REGIONS

REFERENCE ENGINE POWER LEVEL, $Q_o = 4600$ MW

REFERENCE ENGINE RADIATION HEAT FLUX AT EDGE OF FUEL,

$q_o = 2.73 \times 10^{11}$ ERG/CM^2 – SEC

SEE FIG. 5 FOR GEOMETRY AND DIMENSIONS OF REGION OF ANALYSIS

SEE FIG. 6 FOR FUEL, SEED, AND NEON RADIAL PARTIAL PRESSURE DISTRIBUTIONS IN REGION OF ANALYSIS

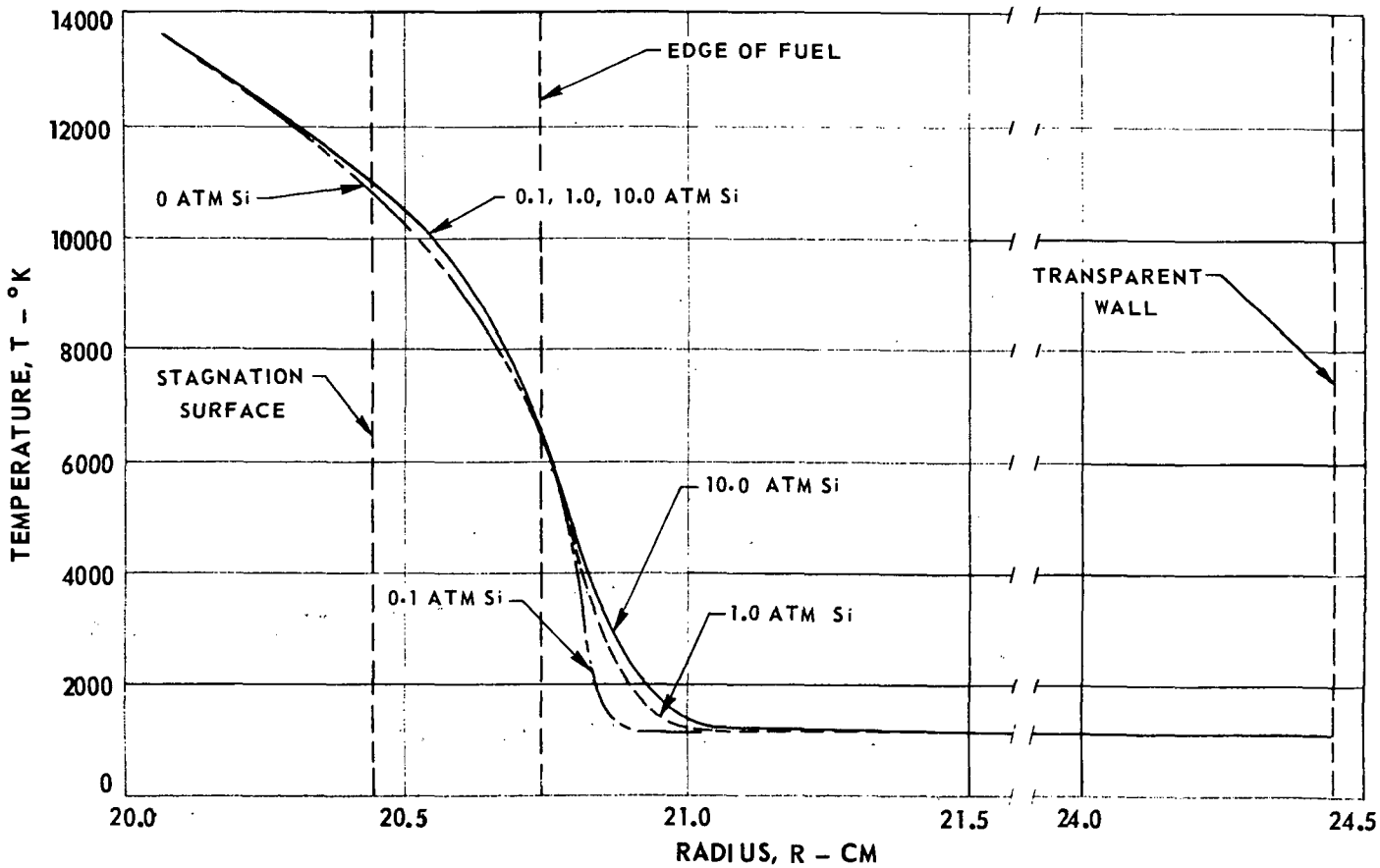

L-910900-16

FIG. 8

FIG. 9

SPECTRAL FLUX EMITTED AT EDGE OF FUEL FOR REFERENCE ENGINE WITH VARIOUS SILICON SEED PARTIAL PRESSURES IN EDGE-OF-FUEL AND BUFFER-GAS REGIONS

REFERENCE ENGINE RADIATION HEAT FLUX AT EDGE OF FUEL, $q_o = 2.73 \times 10^{11}$ ERG/CM^2 - SEC

SEE FIG. 5 FOR GEOMETRY AND DIMENSIONS OF REGION OF ANALYSIS

SEE FIG. 6 FOR FUEL, SEED, AND NEON RADIAL PARTIAL PRESSURE DISTRIBUTIONS IN REGION OF ANALYSIS

SEE FIG. 8 FOR TEMPERATURE DISTRIBUTIONS IN REGION OF ANALYSIS

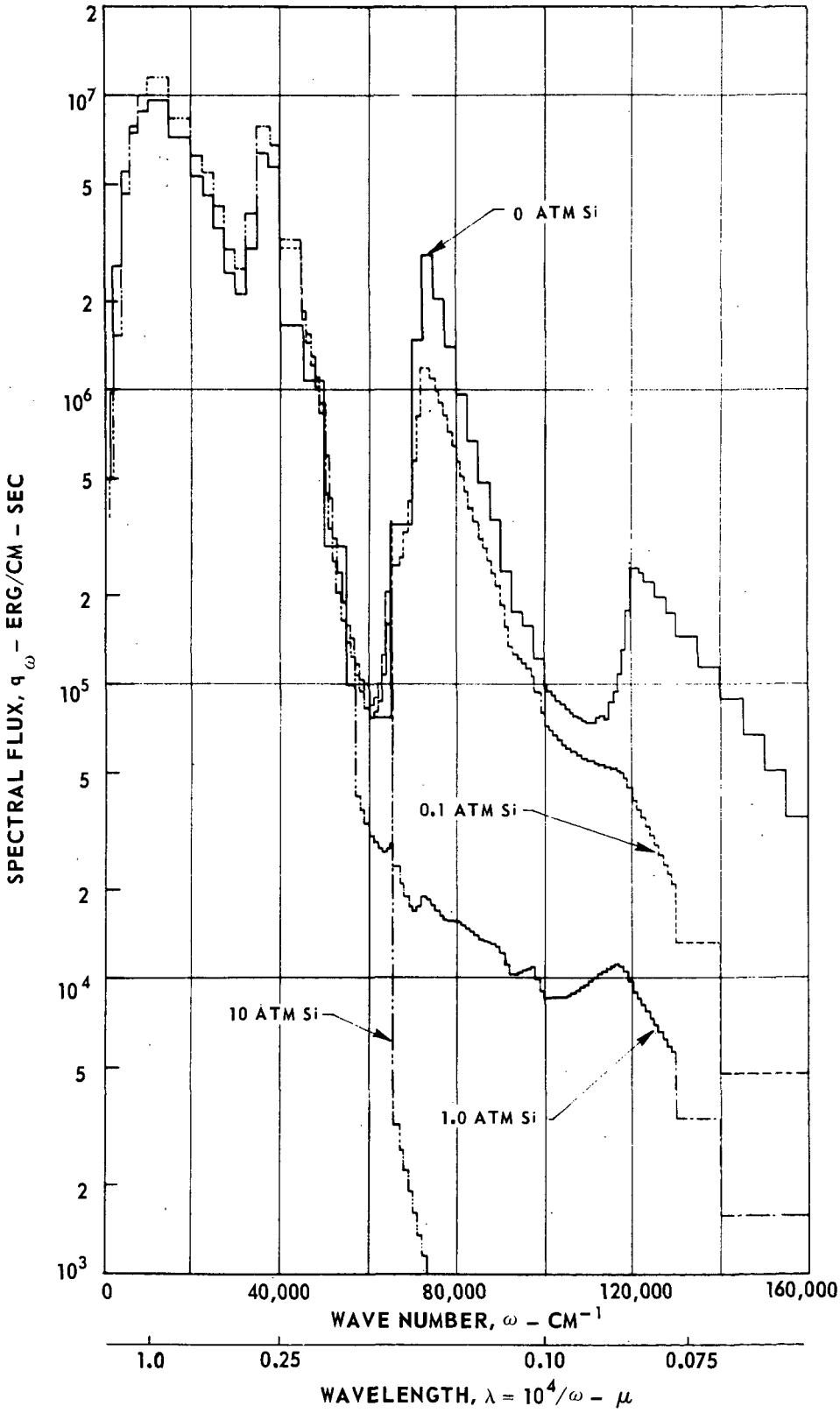

FIG. 10

FRACTIONAL HEAT FLUX DISTRIBUTIONS EMITTED AT EDGE OF FUEL FOR REFERENCE ENGINE WITH VARIOUS SILICON SEED PARTIAL PRESSURES IN EDGE-OF-FUEL AND BUFFER-GAS REGIONS

SEE FIG. 9 FOR CORRESPONDING SPECTRAL FLUX DISTRIBUTIONS

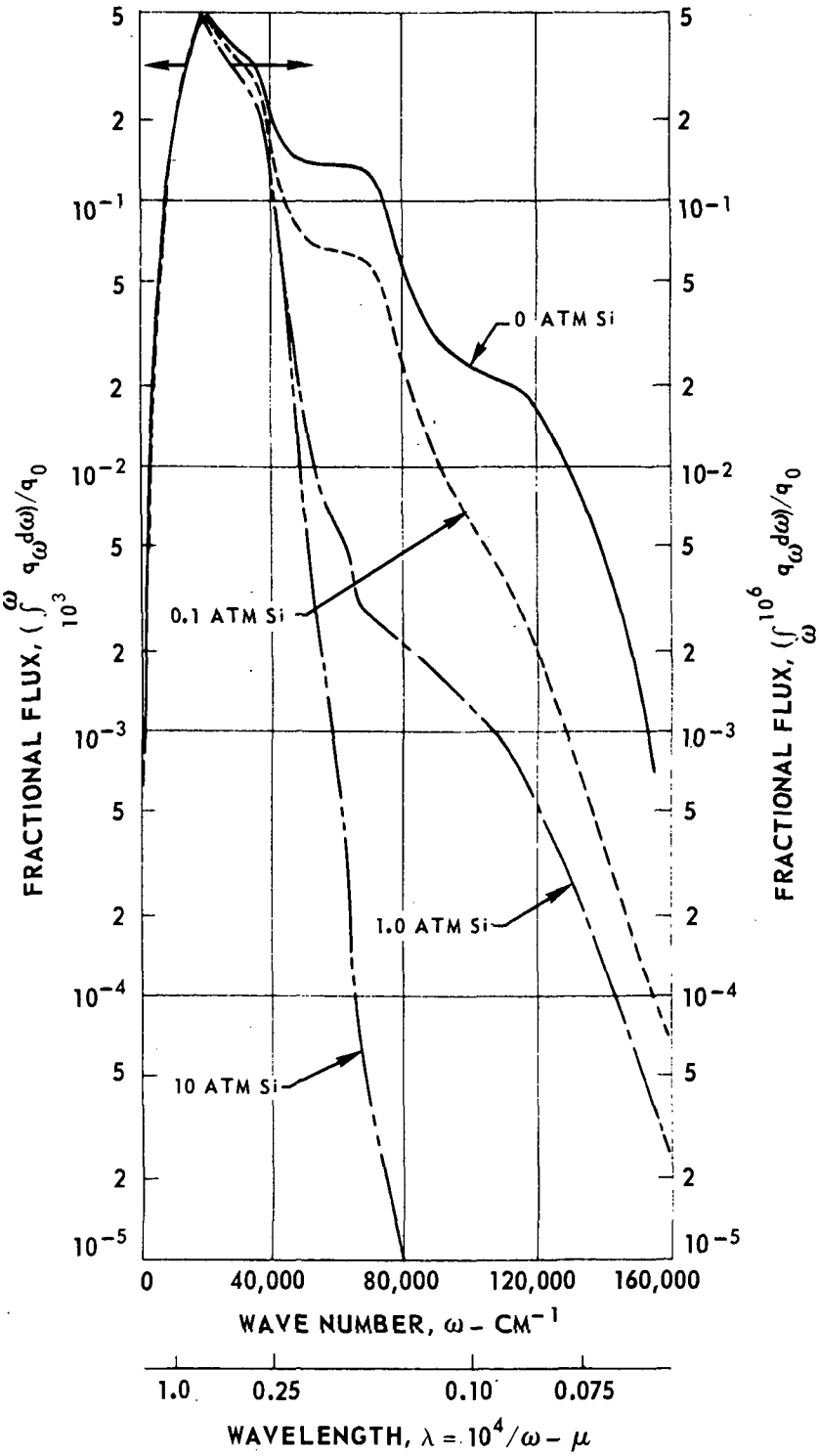

OPTICAL DEPTH DISTRIBUTIONS OF FUEL REGION FOR WAVE NUMBER INTERVAL 75,000 - 72,500 CM^{-1} AT VARIOUS SILICON SEED PARTIAL PRESSURES IN EDGE-OF-FUEL AND BUFFER-GAS REGIONS

REFERENCE ENGINE RADIATION HEAT FLUX, $q_o = 2.73 \times 10^{11}$ ERG/CM^2 - SEC

SEE FIGS. 6 AND 8 FOR PRESSURE AND TEMPERATURE DISTRIBUTIONS

SEE FIG. 9 FOR CORRESPONDING SPECTRAL HEAT FLUX

SILICON ABSORPTION COEFFICIENTS USED ONLY FOR TEMPERATURES LESS THAN ≈10,000°K

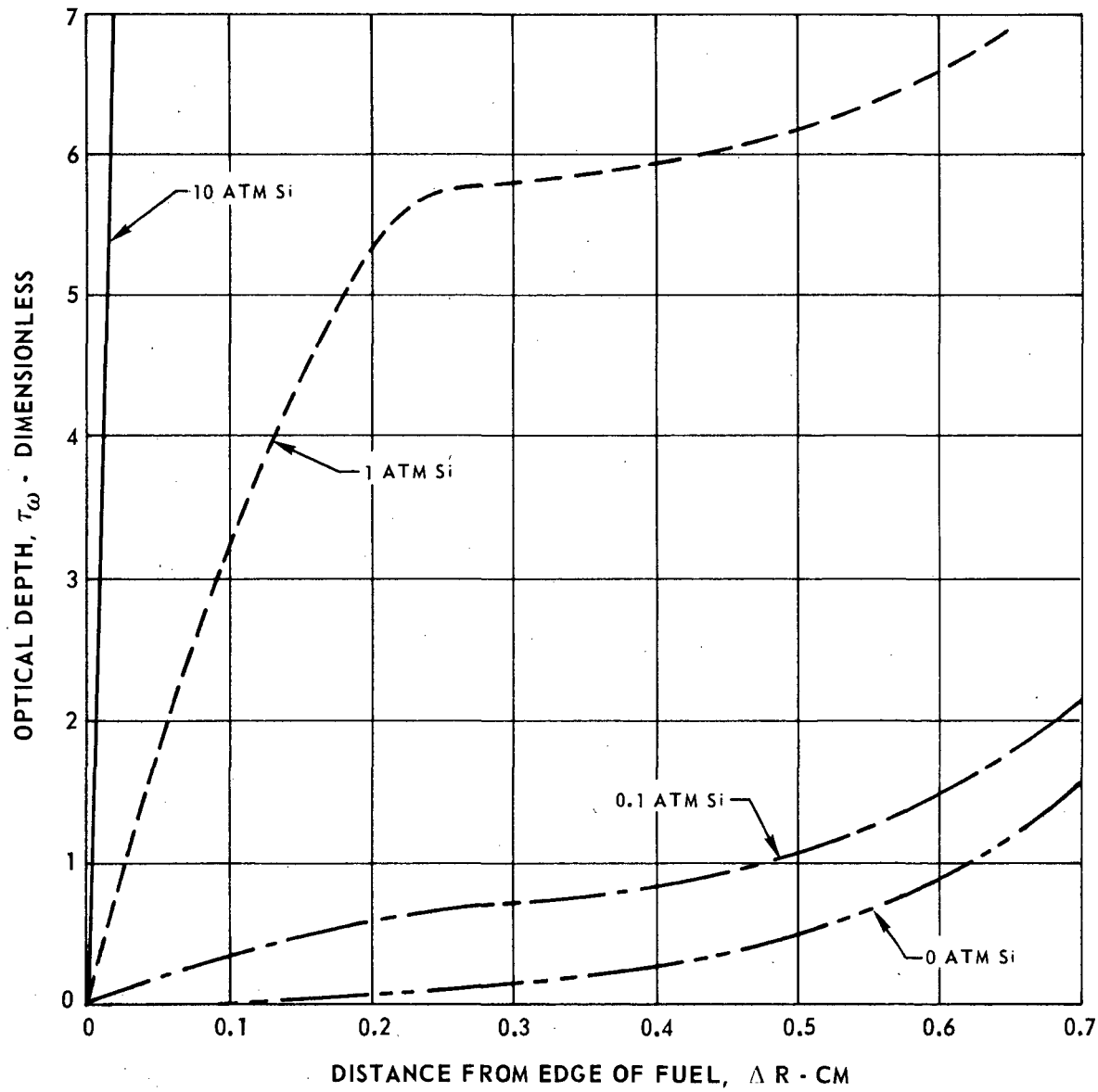

FIG. 12

VARIATION OF EFFECTIVE SPECTRAL BLACK BODY RADIATING TEMPERATURE WITH WAVE NUMBER AT VARIOUS SILICON SEED PARTIAL PRESSURES IN EDGE-OF-FUEL AND BUFFER-GAS REGIONS

REFERENCE ENGINE RADIATION HEAT FLUX, $q_o = 2.73 \times 10^{11}$ ERG/CM^2 - SEC

SEE FIG. 8 FOR TEMPERATURE DISTRIBUTION IN REGION OF ANALYSIS

SEE FIG. 9 FOR CORRESPONDING SPECTRAL HEAT FLUX

T_ω^{bb} DEFINED AS THAT TEMPERATURE FOR WHICH $q_\omega^{bb} = q_\omega^{SEED}$ AT EDGE OF FUEL

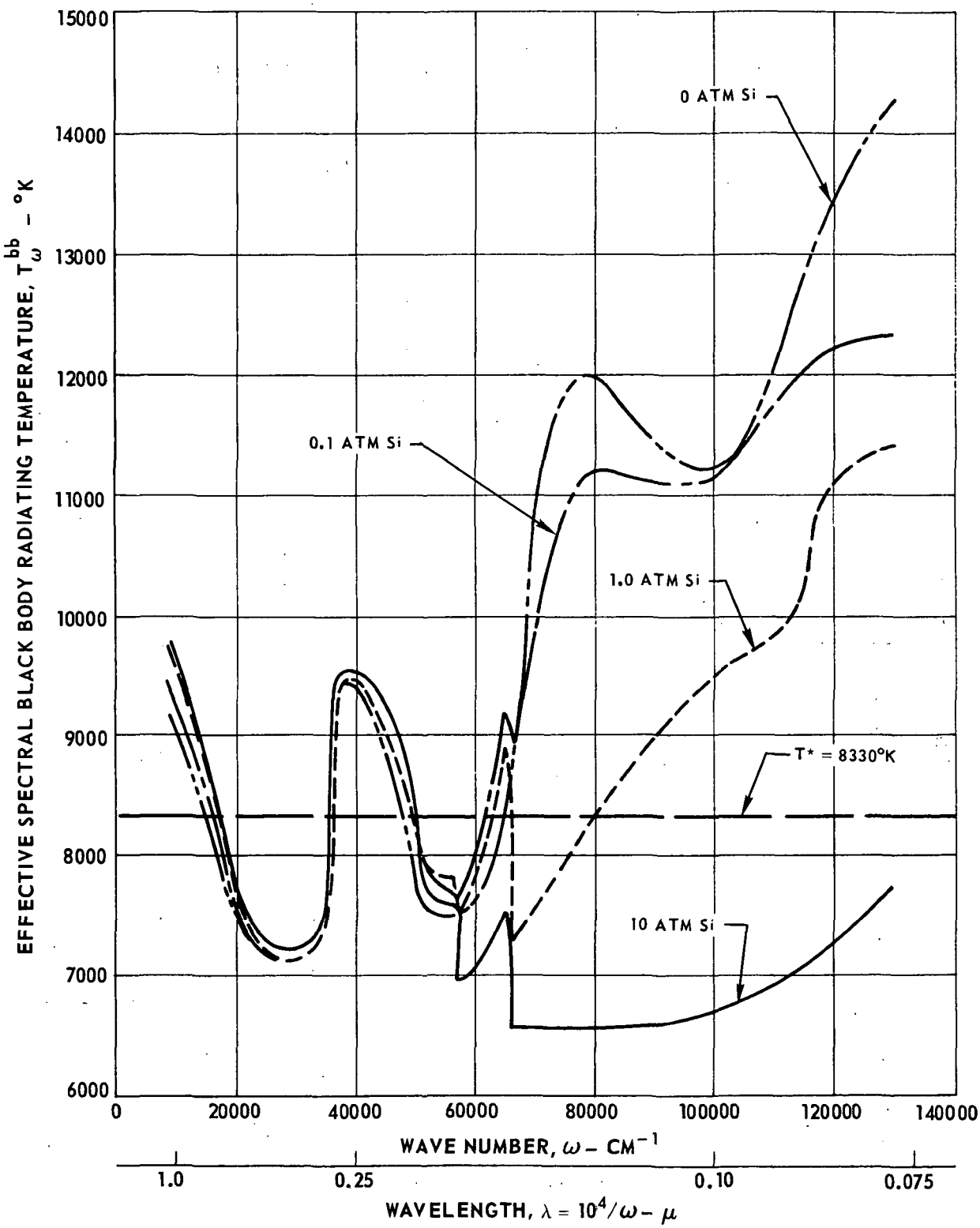

FIG. 13

VARIATION OF INTEGRATED CONVECTED, CONDUCTED, AND NET ABSORBED ENERGY WITH RADIUS FOR REFERENCE ENGINE SEEDED WITH 10 ATM SILICON IN EDGE-OF-FUEL AND BUFFER-GAS REGIONS

Q_{EX} = ABSORBED RADIANT ENERGY - RERADIATED ENERGY

R_{TW} = 24.45 CM

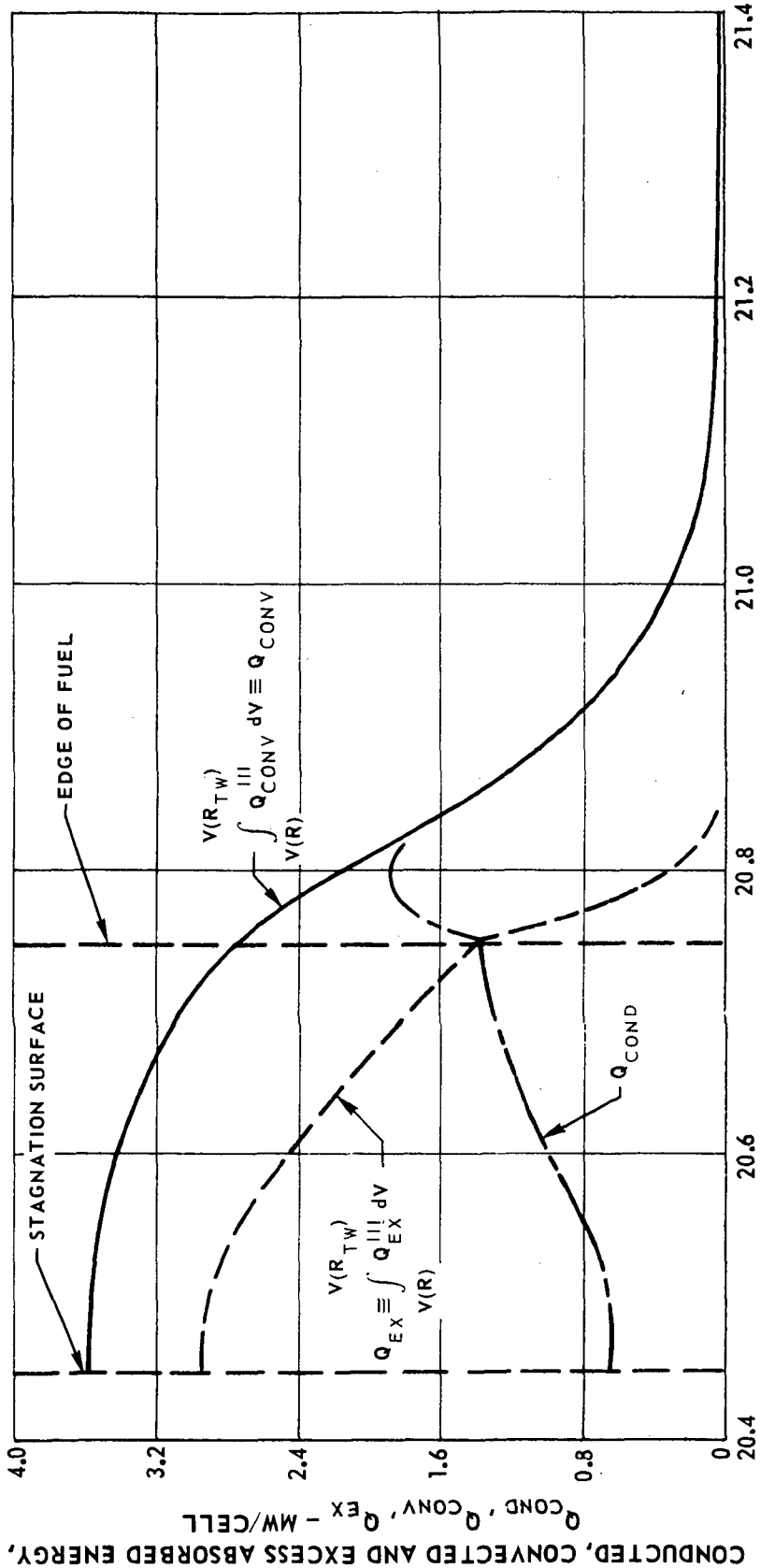

L-910900-16

FIG. 14

RADIAL WEIGHT FLOW AND AXIAL VELOCITY DISTRIBUTIONS BETWEEN ASSUMED RADIAL STAGNATION SURFACE AND TRANSPARENT WALL FOR REFERENCE ENGINE WITH 10 ATM SILICON IN EDGE-OF-FUEL AND BUFFER-GAS REGIONS

$q_o = 2.73 \times 10^{11}$ ERG/CM^2-SEC

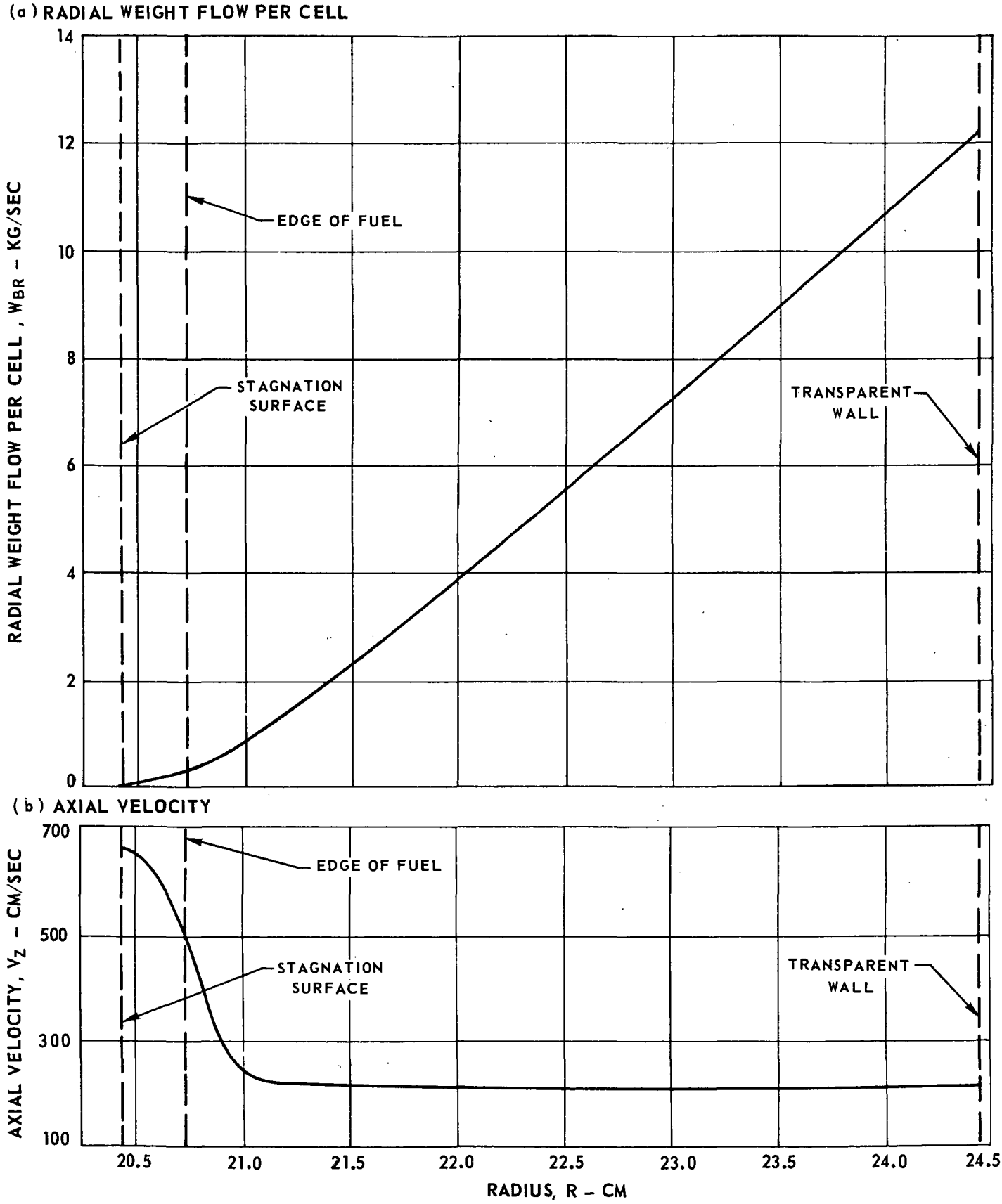

OPTIONAL FLOW CONFIGURATIONS FOR BUFFER-GAS REGION

(a) NEON INJECTION FROM TRANSPARENT WALL WITH AXIAL BYPASS

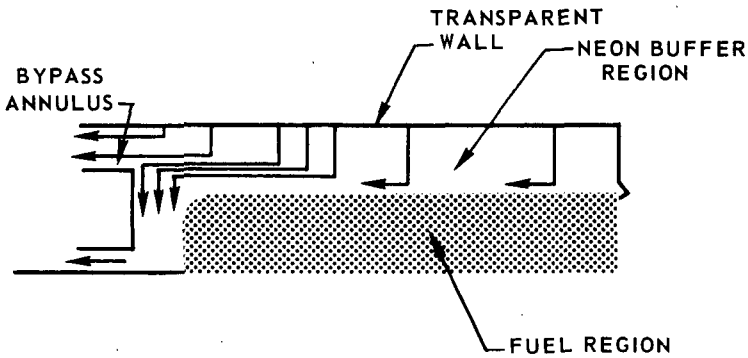

(b) NEON INJECTION FROM TRANSPARENT WALL WITH END-WALL NEON INFLOW

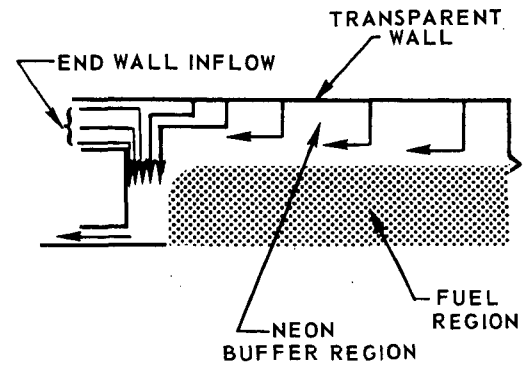

(c) VARIATION OF TOTAL NEON BUFFER WEIGHT FLOW WITH RADIAL LOCATION OF ONSET OF AXIAL BUFFER FLOW

REFERENCE ENGINE SEEDED WITH 10 ATM SILICON

$R_{EOF} - R_{STAG} = 0.30$ CM

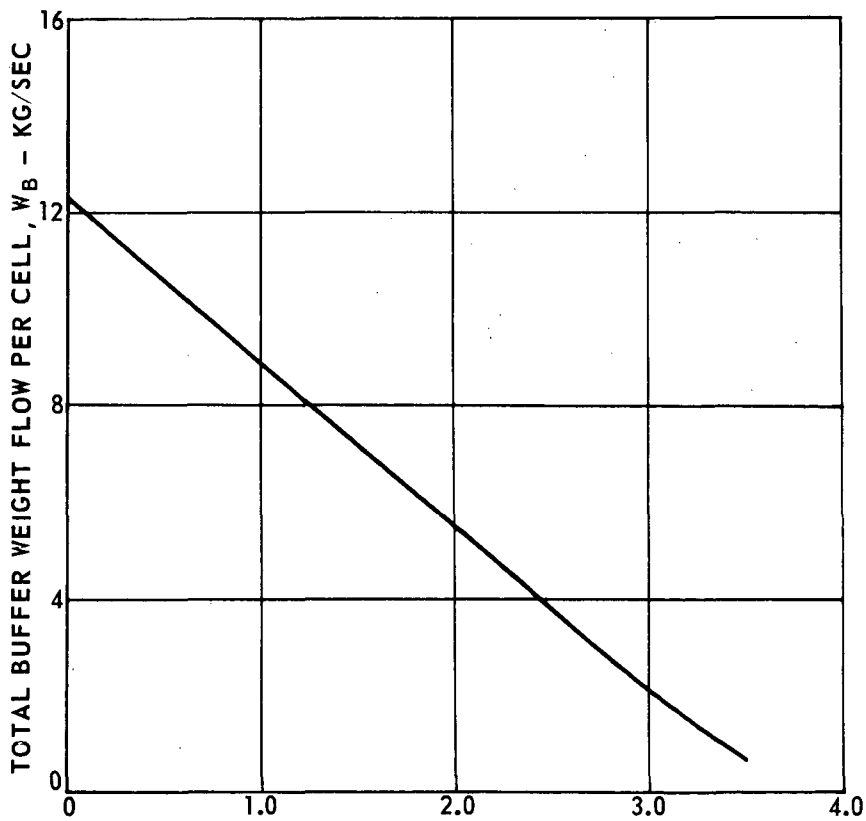

FIG. 16

VARIATION OF BUFFER-GAS MIXED-MEAN TEMPERATURE RISE AND TOTAL WEIGHT FLOW PER CELL WITH LOCATION OF RADIAL STAGNATION SURFACE

REFERENCE ENGINE SEEDED WITH 10 ATM SILICON IN EDGE-OF-FUEL AND BUFFER-GAS REGIONS

$q_o = 2.73 \times 10^{11}$ ERG/CM^2 - SEC

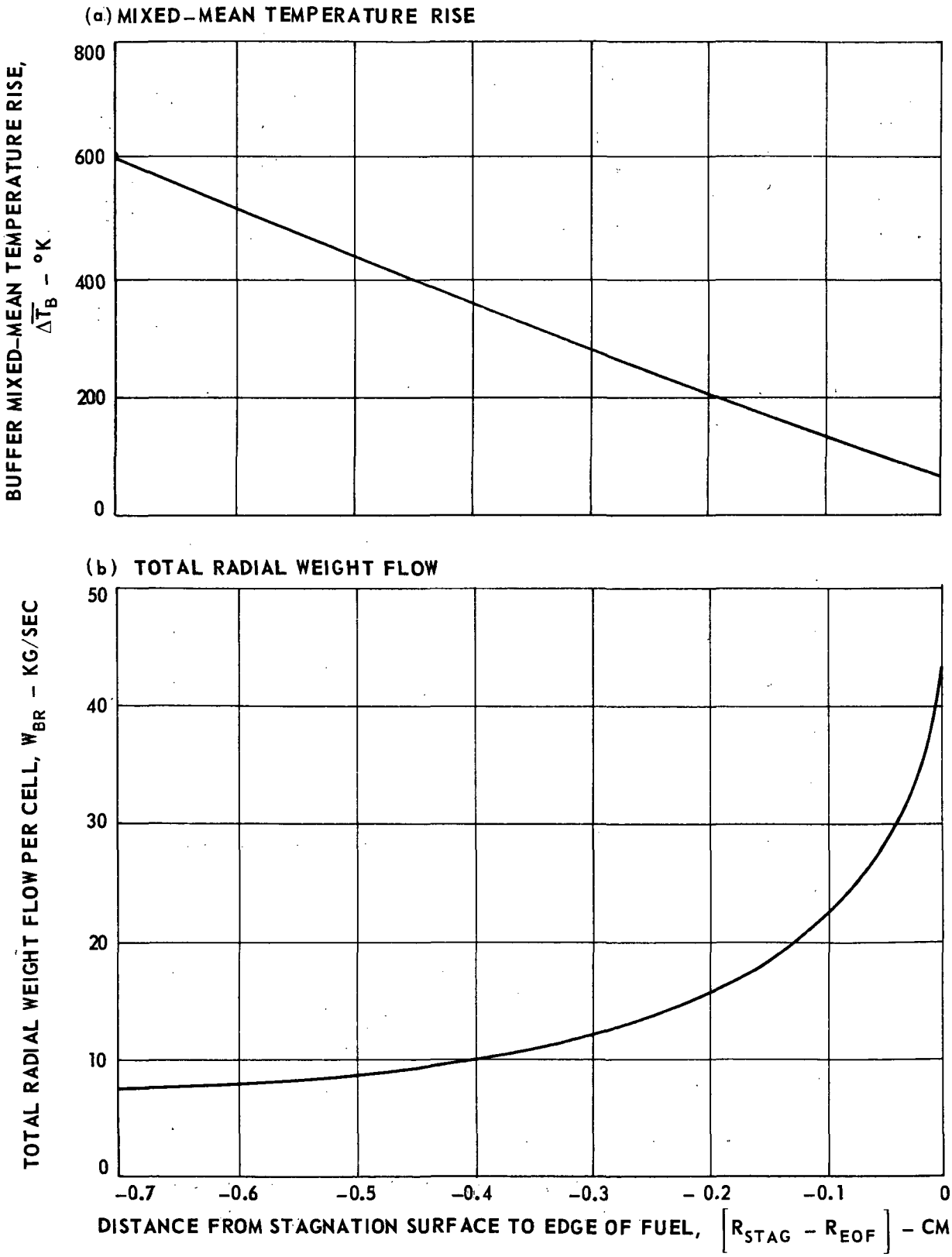

SPECTRAL FLUX AT INNER SURFACE OF TRANSPARENT WALLS FOR REFERENCE ENGINE WITH VARIOUS SILICON SEED PARTIAL PRESSURES IN EDGE-OF-FUEL AND BUFFER-GAS REGIONS

REFERENCE ENGINE RADIATION HEAT FLUX AT EDGE OF FUEL, $q_o = 2.73 \times 10^{11}$ ERG/CM^2 - SEC

SEE FIG. 5 FOR GEOMETRY AND DIMENSIONS OF REGION OF ANALYSIS

SEE FIG. 6 FOR FUEL, SEED, AND NEON RADIAL PARTIAL PRESSURE DISTRIBUTIONS IN REGION OF ANALYSIS

SEE FIG. 8 FOR TEMPERATURE DISTRIBUTIONS IN REGION OF ANALYSIS

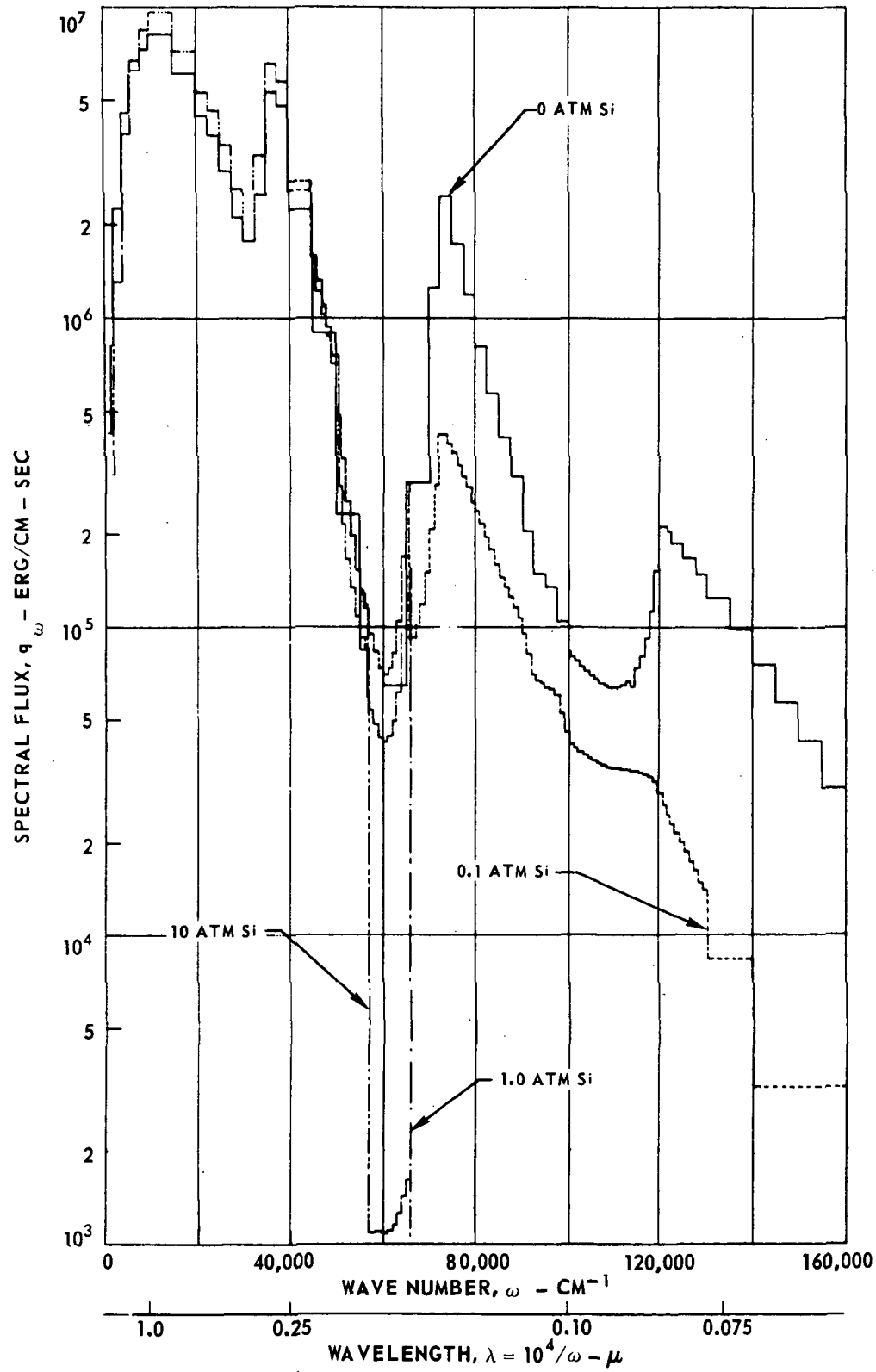

MEASURED TRANSMISSION CHARACTERISTICS OF FUSED SILICA

DATA FROM REF. 30 FOR CORNING 7940 AND THERMAL AMERICAN SPECTROSIL

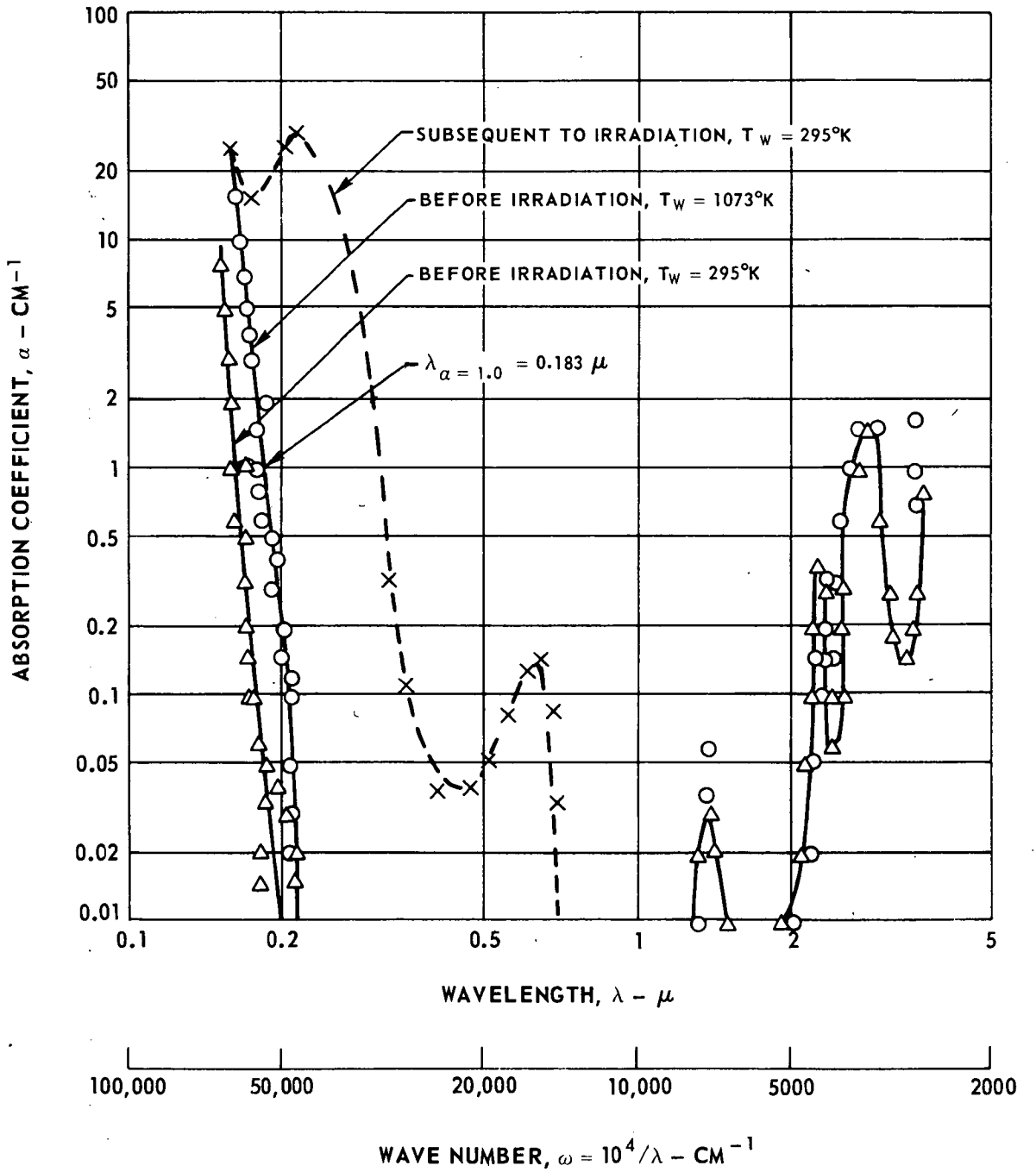

FIG. 19

POWER DEPOSITED IN TRANSPARENT WALLS OF NUCLEAR LIGHT BULB REFERENCE ENGINE RESULTING FROM ABSORPTION OF ULTRAVIOLET RADIATION

ENGINE POWER = 4600 MW

SPECTRAL HEAT FLUX CALCULATED WITH 10 ATM SILICON IN EDGE-OF-FUEL AND BUFFER-GAS REGIONS; SEE FIG. 17

SEE FIG. 18 FOR FUSED SILICA SPECTRAL ABSORPTION COEFFICIENTS

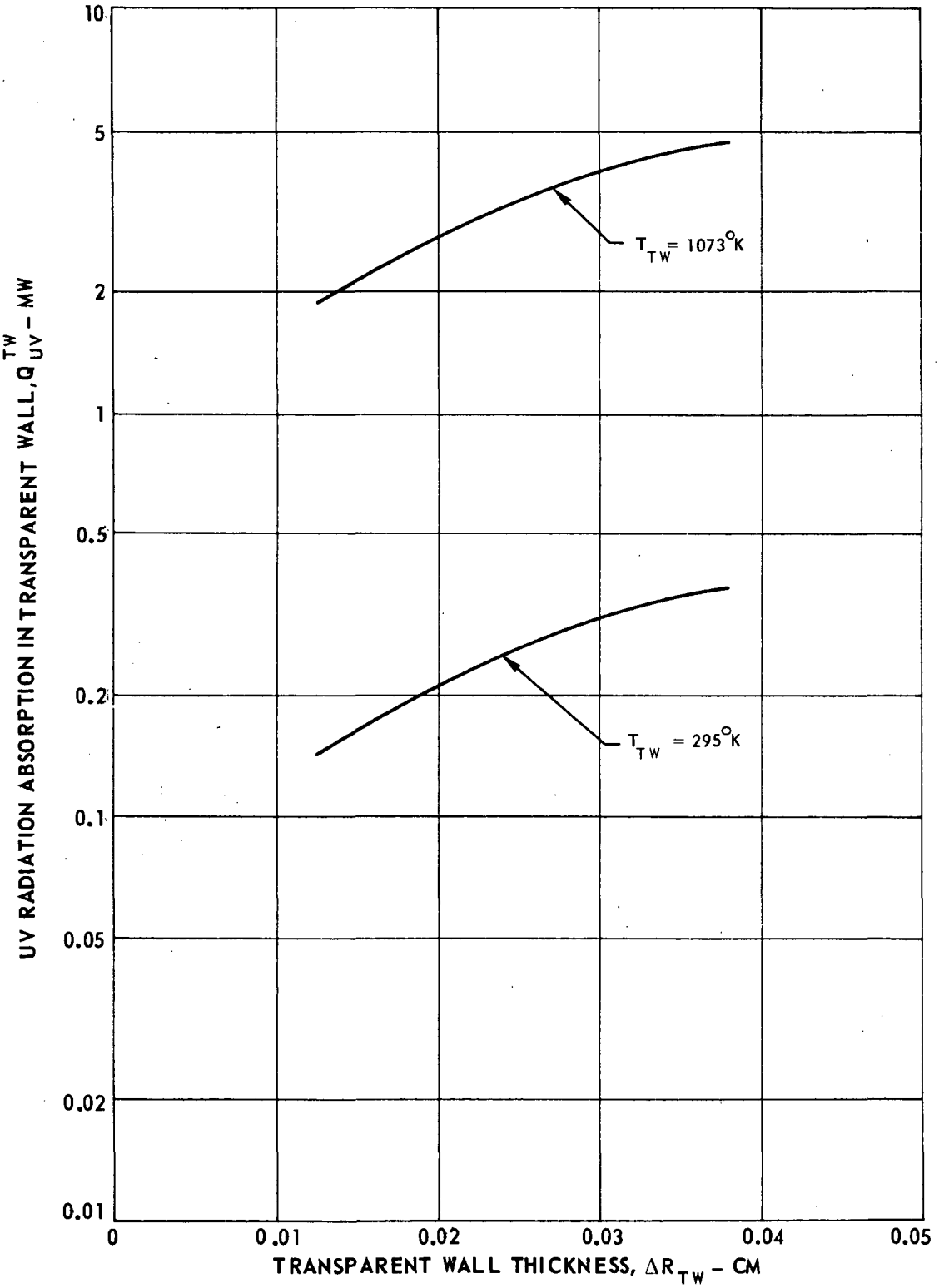

POWER DEPOSITED IN TRANSPARENT WALLS OF REFERENCE ENGINE RESULTING FROM NUCLEAR-RADIATION-INDUCED ENERGY ABSORPTION

ENGINE POWER = 4600 MW

SPECTRAL HEAT FLUX CALCULATED WITH 10 ATM SILICON IN EDGE-OF-FUEL AND BUFFER-GAS REGIONS; SEE FIG. 17

VARIATION OF NUCLEAR-RADIATION-INDUCED ABSORPTION COEFFICIENTS WITH WAVELENGTH AND DOSE RATE TAKEN FROM REFS. 30 AND 31

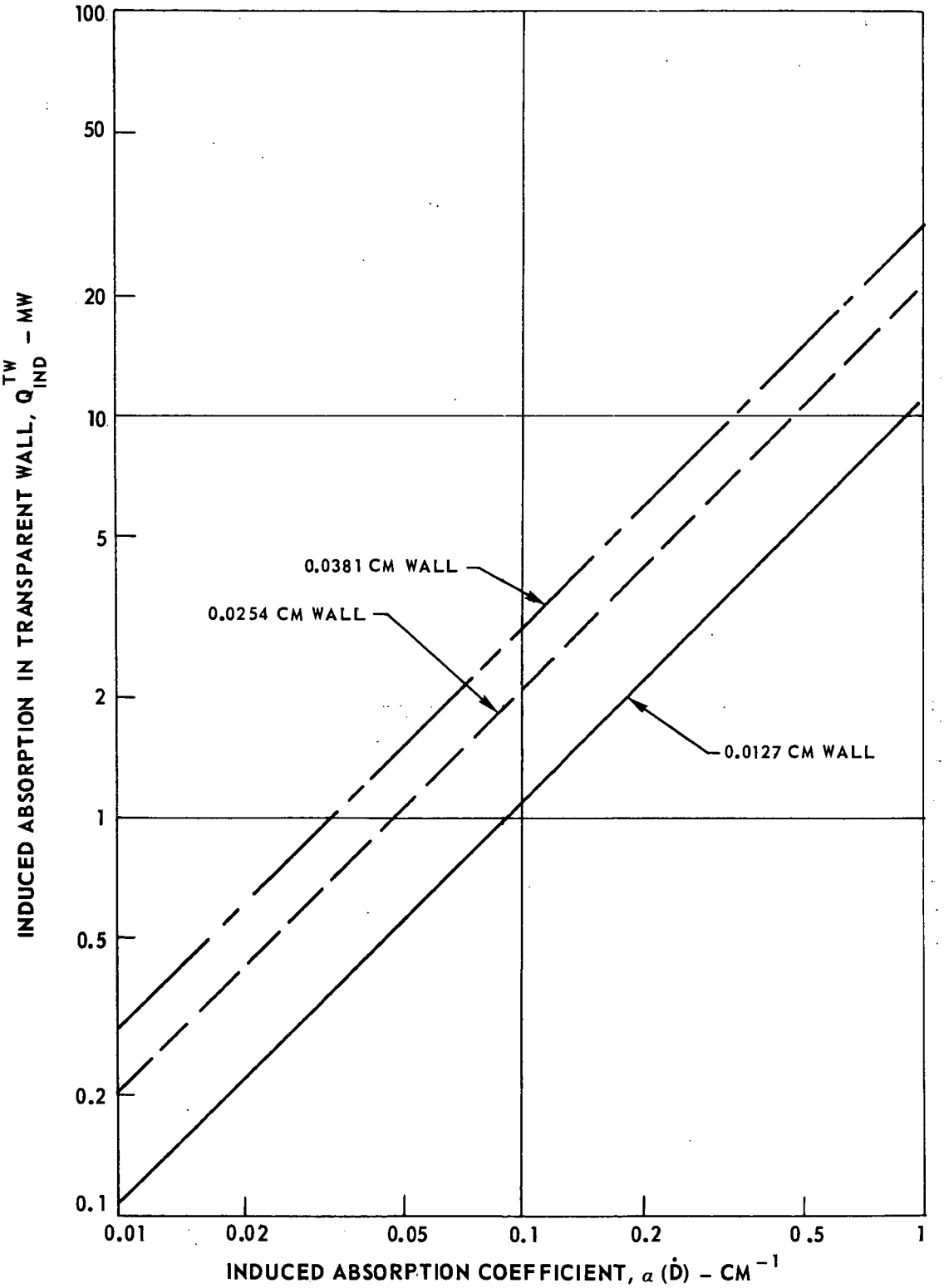

FIG. 21

COMPARISON OF OPTICAL DEPTH DISTRIBUTIONS FOR WAVE NUMBER INTERVAL 75,000 TO 72,500 CM $^{-1}$ FOR INJECTION OF SILICON SEED WITH NUCLEAR FUEL OR WITH NEON BUFFER GAS

SEE FIG.8 FOR TEMPERATURE DISTRIBUTION

SILICON ABSORPTION COEFFICIENTS USED ONLY FOR TEMPERATURES LESS THAN ≈10,000°K

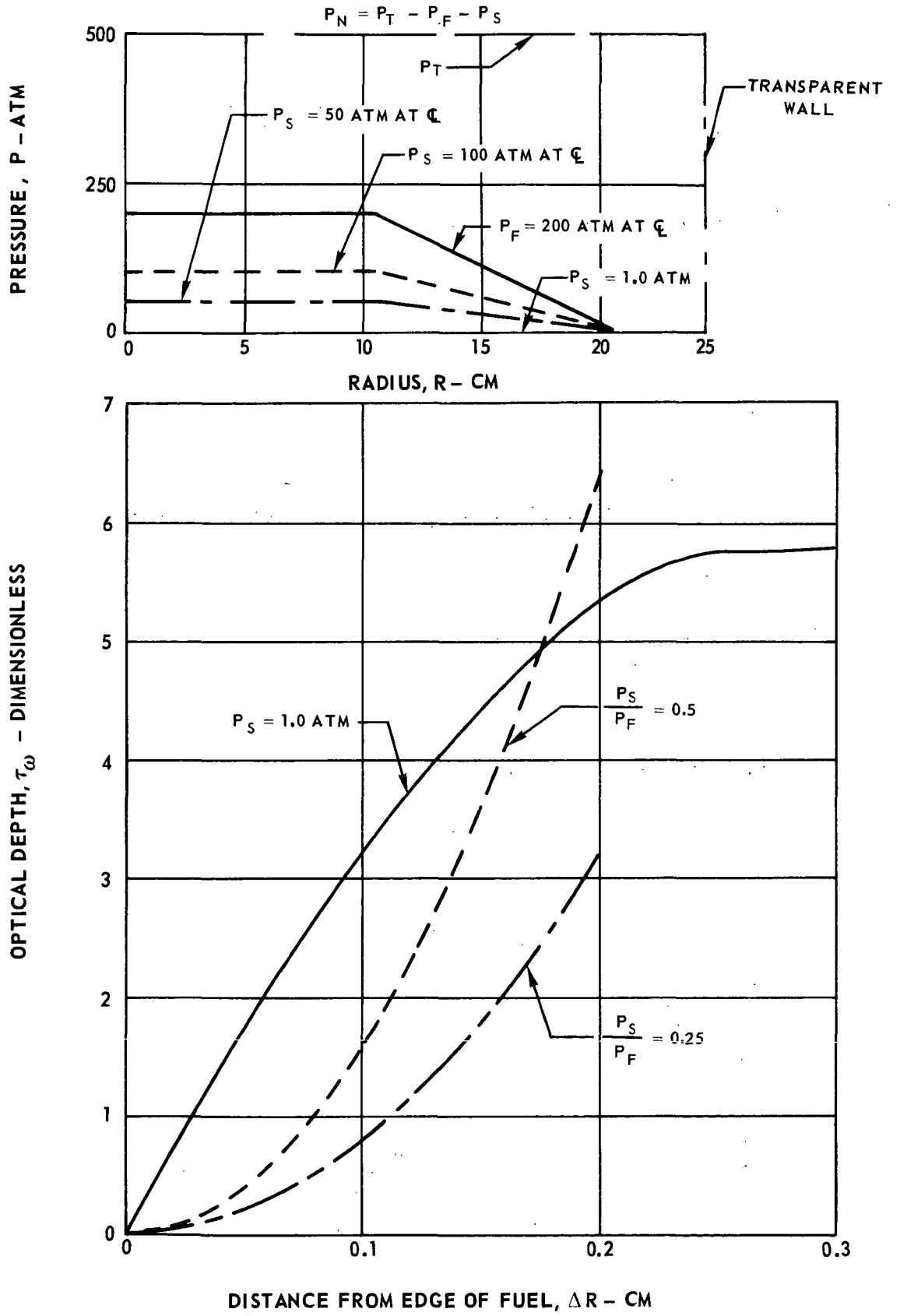

POWER LEVEL RESPONSES OF CONTROLLED ENGINE TO STEP CHANGES IN FUEL INJECTION CONTROL VALVE AREA

$$W_F = K_F A_F \left(\frac{P_I - P_T}{0.25}\right)^{1/2}$$

—— CALCULATED RESPONSE FROM REF. 7

○ SYMBOL INDICATES CALCULATED RESPONSE FOR REVISED REFERENCE ENGINE

(a) INITIAL STEP INCREASE IN CONTROL VALVE AREA

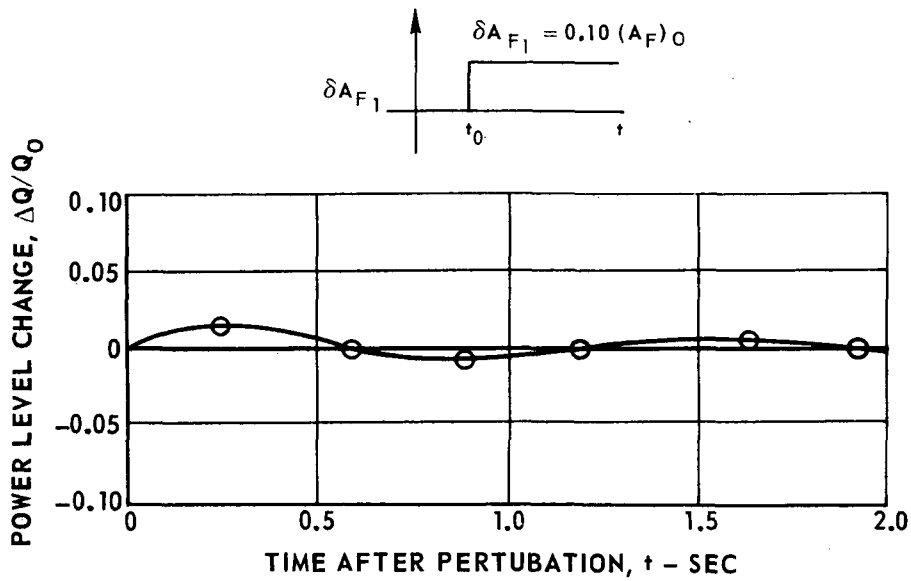

(b) INITIAL STEP DECREASE IN CONTROL VALVE AREA

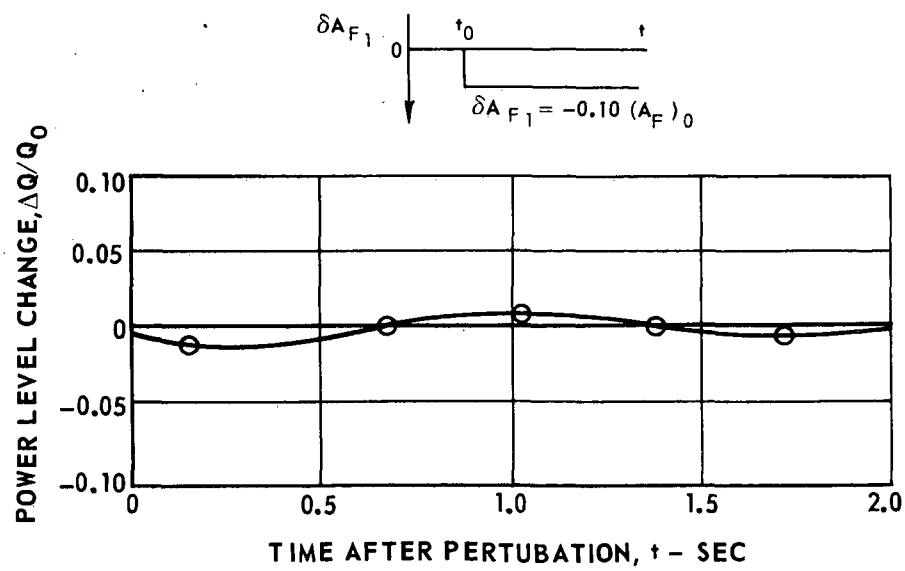

United
Aircraft
Research
Laboratories

UNITED AIRCRAFT CORPORATION

EAST HARTFORD, CONNECTICUT 06108